International Journal of Engineering Science 198 (2024) 104056

Contents lists available at ScienceDirect

International Journal of Engineering Science

journal homepage: www.elsevier.com/locate/ijengsci

Full Length Article

On mechanics of piezocomposite shell structures

Mohammad Malikan

Department of Mechanics of Materials and Structures, Faculty of Civil and Environmental Engineering, Gdańsk University of Technology, ul. Gabriela Narutowicza 11/12, Gdańsk 80-233, Poland

ARTICLE INFO

Keywords:
Smart composite
Piezoceramic
Shells
Bending
Analytical model

ABSTRACT

This study presents an original and novel investigation into the mechanics of piezo-flexo-magneto-elastic nanocomposite doubly-curved shells (PFMDCSs) and the ability to detect the lower and higher levels of electro-magnetic fields. In this context, by utilizing the first-order shear deformation shell model, stresses and strains are acquired. By imposing Hamilton's principle and the von Kármán approach, the governing equations have been obtained. The intelligent shell model consists of size-dependent influences, viz., strain gradients. This will take place via Mindlin's strain gradient elasticity theory and the subsequent re-establishing of the mathematical framework by incorporating this concept. The strain gradient results in a flexoelectric/flexomagnetic effect. The converse effect of the magnetic field on the basis of a close circuit has been assumed. The developed bending equations have been transferred into the algebraic ones by substituting an analytical technique based on homogeneous immovable simple support for the four edges. The problem has been solved according to the Newton-Raphson iteration scheme, and transverse deflections have been computed. For researching the rightness and precision of the shell models together with the solution process, a comparison is prepared by the finite element method (FEM) results for simplified shells, and a good correlation has been observed. At last, by examining several factors governing the problem, the conditions under which the magnetic effects can be noticeable and dominant in doubly-curved shells have been sought. This study could serve as a benchmark reference for piezoceramic-DCSs, as the presented governing equations are original. The most interesting outcome of this research is that the electro-magnetic response of intelligent structures can be entirely geometry-dependent.

1. Introduction

The outstanding strength-to-weight ratio of shells, the most proficient element among engineering structures, has demonstrated remarkable durability. Consequently, various scientific fields have harnessed the potential of shells. When it comes to the configuration of these elements, the design possibilities are limitless, offering an infinite array of shell compounds. From an engineering perspective, shells can be broadly categorized into two groups: shells with developable and non-developable shapes. Developable shells, exemplified by barrel shells, can be flattened without tearing or stretching. On the contrary, the non-developable shells, like double-curvature ones, lack the ability or possibility to be unrolled.

Among the different types of shells, doubly-curved shells (DCSs) are widely used due to their high energy absorption capacity in plastic deformation. DCSs have a very economical design because of their very small thickness-to-span ratio. These structures transfer loads highly efficiently. Because of their curvatures, instead of bending, the forces are transferred in DCSs by membrane forces. In

E-mail addresses: mohammad.malikan@yahoo.com, mohammad.malikan@pg.edu.pl.

https://doi.org/10.1016/j.ijengsci.2024.104056
Received 6 February 2024; Received in revised form 5 March 2024; Accepted 7 March 2024
Available online 12 March 2024

Nomenclature

$u_i(i=1,3)$	Displacements in the α, β, and z- directions
ε_{ij}	Elastic strains
σ_{ij}	Elastic stresses
ψ	External magnetic potential
h_{ijkl}	4th-order converse flexomagnetic tensor
f_{ijkl}	4th-order direct flexomagnetic tensor
C_{ijkl}	4th-order elasticity tensor
$N_{ij}(i,j=\alpha,\beta)$	Force stress resultants
η_{ijk}	Gradient of the elastic strains
$T_{ijk}(i,j,k=\alpha,\beta)$	Higher-order force stress resultants
$R_{ijk}(i,j,k=\alpha,\beta)$	Higher-order moment stress resultants
ξ_{ijk}	Higher-order stress tensor
T_{ij}	Hyperstress resultant
u, v	In-plane displacements of mid-surface along α and β axes
p	Increments in Newton-Raphson method
δ_{ij}	Kronecker's delta
w	Lateral displacement
α	Length coordinate
a	Length of the shell
H_i	Magnetic field
B_i	Magnetic flux
l	Material's length scale parameter
Ψ	Magnetic potential function
m,n	Mode numbers
$M_{ij}(i,j=\alpha,\beta)$	Moment stress resultants
∇	Nabla operator
ν	Poisson's ratio
$\varphi_\alpha,\varphi_\beta$	Shell elements rotations
k_s	Shear correction factor
G	Shear modulus
$Q_{\alpha z}, Q_{\beta z}$	Shear stress resultants
R_α, R_β	Shell radiuses
U	Strain energy
a_{ij}	2nd-order magnetic permeability tensor
g_{ijklmn}	6th-order strain gradient tensor
g_i	Strain gradient coefficients
μ	Strain gradient shear modulus
$a_i(i=1,2,3)$	Surface metrics (tangent vectors)
q_{ijk}	3rd-order piezomagnetic tensor
z	Thickness coordinate
h	Thickness of the shell
q_0	Transverse load
$U_{mn}, V_{mn}, W_{mn}, \Phi_{\alpha mn}, \Phi_{\beta mn}$	Unknown variables for displacements
Δ	Unknown variables vector
$N^0_{ij}(i,j=\alpha,\beta)$	Axial stress resultants of magnetic field
W	Work done by a magnetic field
β	Width coordinate
b	Width of the shell
E	Young's modulus

terms of geometry, they can couple the flexural and membrane responses. Double-curvature shells may be either a section of a dome, sphere or revolution. The double-curvature shape can especially increase structural strength and stability. The study of their bending behavior is necessary for use in cases such as aircraft noses or ballistic missiles. In the case of ballistic missiles, their noses are made of a combination of hemispherical and conical shells that buckle when released and hit the target.

Much work has already been done to estimate the mechanics of DCSs on the nano, micro, meso, and macro scales. Alijani et al. (2011) investigated large amplitude frequencies of a functionally graded (FG) DCS on the basis of Donnell's shallow shell theory and

movable simply supported edges. Tornabene et al. (2012) evaluated natural frequencies of a DCS with anisotropic behavior and solved the model via differential quadrature method (DQM) and generalized eigenvalue solution. The first-order shear deformation shell theory (FSDST) was considered. Fazzolari and Carrera (2014) studied natural frequencies of a DCS made of FG materials (FGM) alongside a sandwich DCS-FGM. A modified quasi-3D kinematic model was generated to carry out the problem. Tornabene et al. (2016) examined a laminated DCS using higher-order shell models exposed to external concentrated line and point forces in order to study its mechanical response. Ghayesh and Farokhi (2017) performed research on microsize DCs to analyze large static size-dependent deflections of the specimen in reference to Donnell's nonlinear shell theory. The microscale influence was calculated concerning a modified couple stress hypothesis. Karami et al. (2019) inspected the effect of porosity on natural frequencies of a nanosize DCS. They capture the size influences based on the nonlocal strain gradient model. Wang et al. (2017) presented a semi-analytical analysis to study natural frequencies of FGM sandwich doubly-curved shells (DCSs) and panels (DCPs). Guo et al. (2018) extended the studies on laminated DCSs in different boundary domains using FSDST and a domain decomposition technique. Amabili (2005) considered large-amplitude vibrations of a DCS embedded in the simply supported edges. The kinematic model came from two different theories, Novozhilov's and Donnell's shell theories. Amabili and Reddy (2010) investigated nonlinear frequencies of a laminated DCS by developing a higher-order shear deformation shell theory. Tornabene et al. (2013) explored natural frequencies of laminated doubly-curved panels and shells by deriving a higher-order equivalent single-layer theory. Tornabene and Bacciocchi (2018) took into account the arbitrarily oriented angular velocities in order to evaluate dynamic stability of a laminated DCS. Karimiasl and Ebrahimi (2019) addressed viscoelastic effect in a sandwich DCS in order to extract the large-amplitude natural frequencies. The sandwich DCS contains magnetorheological layer and a flexible core. Karami and Shahsavari (2020) analyzed a laminated FG-DCS at nanoscale subject to external excitation frequencies. The minutely scaled shells were reinforced with graphene platelets, assuming various patterns. Mehar et al. (2021) studied the eigenvalue thermal stability of DCPs. The shell was strengthened with carbon nanotubes (CNTs). Arefi (2018) presented a study on large static deflections of DCSs at nanosize by taking piezoelectricity effect into account. They nested the shell on an elastic foundation. Kundu and Han (2009) established an investigation on snap through and natural frequencies of laminated DCSs considering external humidity and temperature. Tornabene (2011) applied a two-dimensional generalized DQM (GDQM) to investigate DCSs and DCPs on the basis of FSDT. Bich et al. (2013) employed a semi-analytical technique in order to calculate nonlinear natural frequencies of an eccentrically stiffened FG-DCS. The imperfection was supposed to be a minor deviation of the mid-plane of the shell from its desired and normal position. Viola et al. (2013) discussed on the static response of a laminated DCS and DCP on the basis of a higher-order shear deformations shell model. Tornabene et al. (2014) presented a vibration study on the laminated DCSs and DCPs based on a local GDQM that is an advanced type of GDQM. In another work, Tornabene et al. (2017) presented a novel finite shell element for laminated DCSs to compute natural frequencies. Aminipour et al. (2018) conducted research on wave propagation in anisotropic FG-DCSs in respect to a higher-order shell model. Li et al. (2018b) used a semi-analytical solving method in order to get natural frequencies of laminated DCSs. Sobhy (2018) developed DCSs into advanced laminated materials, including piezomagnetic (PM) faces and FG core, which themselves were reinforced by graphene platelets. The composite structure was placed in a thermal environment. Li et al. (2019) presented a new model of DCSs with non-uniform thickness and researched on its natural frequencies in respect to finite element technique, while the shell was made of FGMs. Arefi and Amabili (2021) studied bending and stability of a Multiphysics-laminate DCS at nanoscale concerning a quasi-three-dimensional elasticity model. The analysis involved piezoelectric effect in addition to piezomagneticity. Zamani (2021) assumed a viscoelastic medium under a laminated DCP and calculated the natural frequencies. Cao et al. (2021) extended studies on FG-DCSs by assessing multi-directional functionality for the FG property. It means the properties of FG was scrutinized along with not only thickness but also length and width of the DCS. Tornabene et al. (2021b) presented new research on anisotropic DCSs based on isogeometric mapped geometry and a variable thickness. A higher-order elasticity model was utilized as well. Karimiasl et al. (2019a) researched on the large amplitude frequencies of composite DCSs containing a porous core and piezoelectric layers with multiscale modeling. Tornabene (2019) calculated critical rotational speed of a DCS manufactured by FGMs. The rotational movement was possible to be in an arbitrarily axis. Arefi (2020) carried out a multiphysics vibration analysis on DCSs at small scale consisting of electro-elastic features. They contributed the influence of two-parameter elastic matrix into the model. The nanoscale impacts were captured with respect the Eringen's nonlocal elasticity theory. Thakur and Ray (2021) investigated transient response of a laminated DCS. The shell was subjected to a pulse loading and a higher-order elasticity model was employed to simulate the displacements. Zhu et al. (2021) studied the effect of non-uniform electric field on the natural and excitation frequencies of piezoelectric DCSs comprising porosities. In another work, Tornabene et al. (2021a) assumed a honeycomb core and modeled a laminated DCS based on a higher-order elasticity framework. Lotfan et al. (2021) provided a study on the axially moving DCSs and DCPs in a vibrational environment using a higher-order kinematic model. Civalek (2005) combined finite difference method with a harmonic differential quadrature technique as a unique solution in order to calculate large amplitude frequencies of an isotropic DCS positioned on an elastic matrix. Tsai et al. (2008) modeled a smart FG-DCS with three-dimensional elasticity. The model incorporated electro-magnetic properties. Duc et al. (2019) described large dynamic amplitudes of a nanosize FG-DCS reinforced with carbon nanotubes. The nanocomposite was postulated to be geometrically imperfect and embedded in a thermal environment. Tornabene (2015) used higher-order theories in order to peruse natural frequencies of laminated DCPs. The panel was reinforced by curvilinear fibers. The theoretical model was solved within the context of a local GDQ. Askari et al. (2020) developed studies on vibrations of DCPs including bimorphs and unimorph layouts. Li et al. (2018a) reported nonlinear transient behavior of composite FG-DCSs on the basis of presenting a new kinematic displacement field. Mahapatra et al. (2016) analyzed nonlinear static deflections of a laminated DCS/DCP while the member was affected by external humidity and temperature. Zhu et al. (2019) affected a piezoelectric FG-DCSs by viscosity and surface effects and computed nonlinear frequencies. As this article is not a review paper to give all the literature in detail, some works have been surveyed only. Other published works on doubly-curved shells/panels can be referred as (Tornabene et al., 2012; Ghavanloo & Fazelzadeh, 2013; Huang & Qiao, 2020; Monge & Mantari,

2020; Aminipour et al., 2020; Ahmadi et al., 2021; Vinyas & Harursampath, 2020; Sayyad & Ghugal, 2021; Singh & Panda, 2014; Tornabene & Brischetto, 2018; Arefi & Rabczuk, 2019; Arefi et al., 2022; Shahmohammadi et al., 2022; Bidgoli et al., 2022; Karami et al., 2020; Hao et al., 2018; Fazelzadeh et al., 2019; Zare Jouneghani et al., 2017; Karimiasl et al., 2019b; Tham et al., 2019; Liew & Lim, 1996; Mahapatra et al., 2017a, 2017b; Pouresmaeeli & Fazelzadeh, 2016; Singh & Panda, 2017; Dindarloo et al., 2020; Thakur et al., 2017; Tornabene & Viola, 2013; Tornabene, 2016; Tran et al., 2018; Tornabene et al., 2023; Sofiyev, 2023; Xu et al., 2021; Dastjerdi et al., 2020a;2020b; Dastjerdi et al., 2021a, 2023a;2023b; Khaniki & Ghayesh, 2023; Shahmohammadi et al., 2023).

Under the impact of an external magnetic field, multiferroic materials could exhibit extraordinary properties. These materials are not solely magnetized by an external magnetic field but rather by mechanical deformation. These structures become magnetized by responding to mechanical strain, resulting in the generating of a magnetic field. This lower-level magneto-elastic phenomenon is called piezomagnetism. Examples of multiferroic materials include nickel, cobalt, and iron, as well as certain types of compounds and nanostructures. It is crucial to understand the magneto-elastic behavior of such materials, helping in the development of precision technologies ranging from electro-magnetic micro motors and data storage systems.

A higher-level multiphysics impact, flexomagnetic (FM) influence, is an innovative finding in the realm of small-scale devices. FM materials are often multiferroic, meaning they undergo both ferromagnetic and ferroelastic properties, allowing them to couple magnetic and mechanical behavior. It was shown that the FM is a linear phenomenon arising from the nonuniform strain along the thickness (Lukashev & Sabirianov, 2010). It means that this effect can be absent for a uniform strain. However, it is significant to underline that the FM does not result from the strain. It results from strain gradient along with the thickness. Thus, a nonuniform strain generates a strain gradient and then the strain gradient creates the FM influence. This process gives the direct FM effect. In order to access the converse FM effect, the need is to possess a gradient of the external magnetic field.

In continue, the last research that has focused on the mechanical behavior of piezomagnetic beams and plates by investigating FM impact is elaborated. Forerunners are Sidhardh and Ray (2018) and Zhang et al. (2019). In these early examinations, the researchers concentrated on linear bending of size-dependent actuators and sensors based on a surface elasticity approach and Euler-Bernoulli beam model under a transverse static loading, in which the FM effect is observed in both direct and converse magnetizations. Alternatively, Malikan and Eremeyev (2020a) continued the studies by conducting a frequency examination of the piezomagnetic-flexomagnetic (PFM) one-dimensional structures on the basis of nonlocal thin beam. Malikan and Eremeyev (2020b) performed nonlinear frequencies of small-size structures with PFM properties. Malikan and Eremeyev (2020c) assessed large deformations for a nonlocal beam with the PFM impact. The evaluation has been accomplished by way of a semi-analytical solving technique. Malikan et al. (2020c) explored nonlinear buckling of piezo- and flexomagnetic nanoparticles. Malikan et al. (2020b) considered the size effect and studied a nonlocal PFM beam by encompassing material imperfection. Malikan and Eremeyev (2021a) conducted a research to estimate if there is any dependency between the FM effect and surface elasticity. Malikan and Eremeyev (2021b) reported flexomagnetic behavior for nonlocal sheets. Malikan et al. (2021) modeled a micro media to examine the distribution of temperature in PFM micro beam. Sladek et al. (2021) probed FM effect into cantilever beams subjected to lateral point load and under direct magnetic impact. Malikan and Eremeyev (2022a) tried to explore the shear deformation influences on the FM response of an axially compressed small-size beam. Malikan et al. (2022) addressed FM influence in small size beams made of FGM faced with thermal buckling. Malikan and Eremeyev (2022b) considered the rotary inertia resulted from shear deformations on the mechanical response of flexomagnetic beams. Momeni-Khabisi and Tahani (2023) investigated both direct and converse magnetic effects leading to modelling nano-sensors and nano-actuators for piezomagnetic nanoplates under thermal stability circumstances. Malikan and Eremeyev (2023) modeled FM microbeams using the Lord-Shulman thermoelastic model and studied thermoelastic behavior of piezomagnetic structures in thermo-dynamic conditions. Malikan and Eremeyev (2022c) developed the FM model and proposed a more consistent FM constitutive model. Hrytsyna et al. (2022) analyzed both flexoelectric and flexomagnetic influences simultaneously along with micro-inertia property to study love waves propagation in structures. A continuum conical small size shell made of functionally graded compositions consisting of flexomagnetic and flexoelectric properties has been scrutinized by Dehkordi and Tadi Beni (2022). Very recently, Malikan et al. (2023) derived a three-dimensional (3D) magneto-elastic model for intelligent structures and indicated that the three-dimensional analysis shows different results for such smart structures, indicating the significance of 3D mechanical studies. Biswas and Sahu (2023) studied plane wave characteristics in PFM microstructures. Their study incorporated impedance boundary conditions and micro-inertia effects. Fu et al. (2023) with the inclusion of expanded strain gradient terms inside the free energy density, presented an extended PFM model. Momeni-Khabisi and Tahani (2024) analyzed both buckling and post-buckling of smart nano-strips providing flexoelectric and flexomagnetic influences simultaneously. Biswas and Sahu (2024) continued research on PFM structures adding surface effects while the substrate is under plane waves.

The present work, as investigated the literature, is the first endeavor to estimate the FM in a shell structure. This work is prepared regarding some aspects. First of all, the presentation of the new modified PFM relationships for a two-dimensional structure. In this way, a third part is involved which was absent in the stress-displacement piezo-flexo-magneto-elastic relations of the literature. In addition to this, magnetic induction-type tensor is also involved as a new part in the formulation, which was excluded from past researches. In this way, both magnetic vector and tensor are engaged. The second is the analysis of doubly-curved shells in the form of a PFM shell, which in turn is novel. This work shows that how flexomagneticity can operate in a PFMDCS. The assumptions to evaluate the problem consist of the first-order shear deformation shell model (FSDST) beside the von Kármán theory. FSDST describes the geometry of shell after deformations. The formulation of linear bending requires linear Lagrangian strains. The third and final aspect is the use of an analytical solution method in order to transfer the partial differential equations of bending into the space of algebraic equations, leading to an analytical solution.

The organization of the paper unfolds as follows:

In Section 1, the focus is on introducing the topic alongside a comprehensive review of the existing literature. Section 2 entails the

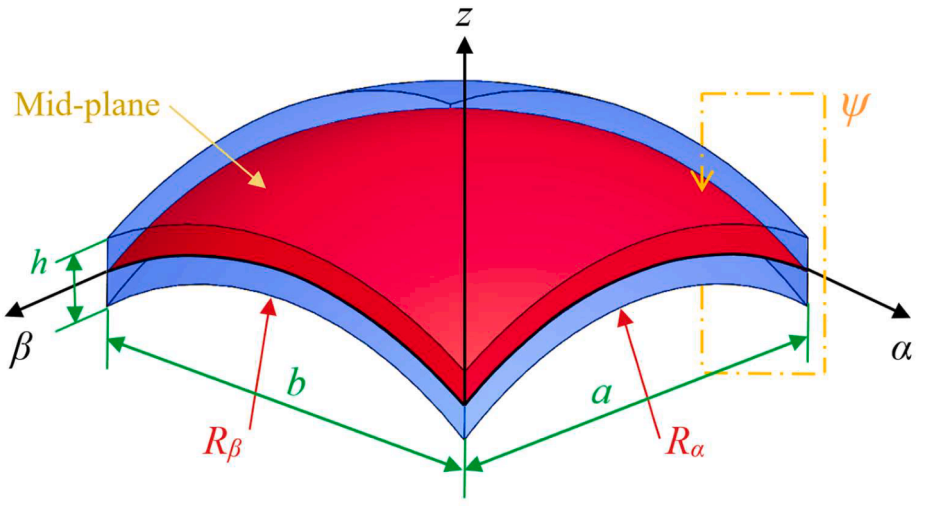

Fig. 1. Doubly-curved shells of revolution (designed in SolidWorks 2023).

mathematical modeling of the targeted issue. By Section 3, the analytical solution process is outlined. Section 4 undertakes some comparative analyses in accordance with FEM. Turning to Section 5, a thorough examination and detailed interpretation of the results are presented. Finally, Section 6 encapsulates the paper, providing conclusive remarks and summarizing the key findings of the conducted research.

2. Mechanics of PFMDCSs

This section represents the mechanics of PFMDCSs by virtue of a well-derived mathematical model. By means of analytical mathematics, the mechanics of the studied shell is explained. Moreover, the PFMDCSs failure is analyzed in regard to the lateral loads. The main attention is paid to the piezomagnetic and flexomagnetic behavior of PFMDCSs. In this work, a DCS is considered with equal curvatures on both sides, which is layup by Fig. 1. As seen, the letters *a, b*, and *h* are respectively associated to the length, width, and thickness of the PFMDCS. The shell is conjugated to a magnetic field which acts transversely and a curvilinear coordinate system is attached to the domain. R_α and R_β denote the principal radii of the curved dimensions.

As it is obvious from Fig. 1, the actual geometric shapes of the DCSs are specified by curvatures R_α and R_β. Practical engineering has often encountered through several geometrical shapes of DCSs, i.e. catenary, hyperbolical, elliptical shells, paraboloid, cycloidal, circular cylindrical, circular saddle, circular toroidal, etc. Despite that, in the context of brevity, this study is supposed to investigate a few of them only.

In accordance with the postulates outlined in the relatively thick shell hypothesis mentioned earlier, the kinematic field for an arbitrary point of the shell analyzed in the present research adheres to the first-order shear deformation shell theory, which could be expressed as follows (Pouresmaeeli & Fazelzadeh, 2016; Reddy & Asce, 1984; Reddy, 2003; Reddy & Liu, 1985):

$$\begin{Bmatrix} u_1(\alpha,\beta,z) \\ u_2(\alpha,\beta,z) \\ u_3(\alpha,\beta,z) \end{Bmatrix} = \begin{Bmatrix} \left(1+\frac{z}{R_\alpha}\right)u(\alpha,\beta) \\ \left(1+\frac{z}{R_\beta}\right)v(\alpha,\beta) \\ w(\alpha,\beta) \end{Bmatrix} + z\begin{Bmatrix} \varphi_\alpha(\alpha,\beta) \\ \varphi_\beta(\alpha,\beta) \\ 0 \end{Bmatrix} \tag{1}$$

Let us utilize the conventional linear Lagrangian strain-displacement formula as follows:

$$\varepsilon_{ij} = \frac{1}{2}\left(\frac{\partial u_i}{\partial x_j} + \frac{\partial u_j}{\partial x_i}\right) \tag{2}$$

The tensors representing strain and strain gradients exhibit symmetry in this context as $\varepsilon_{ij} = \varepsilon_{ji}$ and $\eta_{ijk} = \eta_{jik}$. Then, the progress continues with the expansion of Eq. (2) for an orthogonal curvilinear coordinate system (Dindarloo et al., 2020; Reddy & Asce, 1984; Reddy, 2003):

$$\left\{\begin{array}{c}\varepsilon_{\alpha\alpha}\\ \varepsilon_{\beta\beta}\\ \gamma_{\beta z}\\ \gamma_{\alpha z}\\ \gamma_{\alpha\beta}\end{array}\right\}=\left\{\begin{array}{c}\frac{1}{A_1}\left(\frac{\partial u_1}{\partial\alpha}+\frac{1}{a_2}\frac{\partial a_1}{\partial\beta}u_2+\frac{a_1}{R_\alpha}u_3\right)\\ \frac{1}{A_2}\left(\frac{\partial u_2}{\partial\beta}+\frac{1}{a_1}\frac{\partial a_2}{\partial\alpha}u_1+\frac{a_2}{R_\beta}u_3\right)\\ \frac{1}{A_2}\frac{\partial u_3}{\partial\beta}+A_2\frac{\partial}{\partial z}\left(\frac{u_2}{A_2}\right)\\ \frac{1}{A_1}\frac{\partial u_3}{\partial\alpha}+A_1\frac{\partial}{\partial z}\left(\frac{u_1}{A_1}\right)\\ \frac{A_2}{A_1}\frac{\partial}{\partial\alpha}\left(\frac{u_2}{A_2}\right)+\frac{A_1}{A_2}\frac{\partial}{\partial\beta}\left(\frac{u_1}{A_1}\right)\end{array}\right\}\tag{3}$$

in which $A_1=\left(1+\frac{z}{R_\alpha}\right)a_1, A_2=\left(1+\frac{z}{R_\beta}\right)a_2, A_3=a_3=1$.

In order to derive strain-displacement relations, one may assume the following criteria (Aminipour et al., 2018),

1) The shallow shell is taken into account, and then thickness deformation is considered insignificant compared to the curvature radii

$$(\partial/\partial z=0)=:\left\{\begin{array}{l}\frac{z}{R_\alpha}\approx 0\Rightarrow A_1=a_1\\ \frac{z}{R_\beta}\approx 0\Rightarrow A_2=a_2\end{array}\right.$$

2) It is supposed that the curvatures are constant and do not have variations: $\frac{\partial a_1}{\partial\beta}=\frac{\partial a_2}{\partial\alpha}=0$

Next, one can articulate the strain components at any point on the domain by elaborating and segmenting them as (Arefi & Rabczuk, 2019):

$$\left[\begin{array}{ccc}\varepsilon_{\alpha\alpha} & \gamma_{\alpha\beta} & \gamma_{\alpha z}\\ \gamma_{\alpha\beta} & \varepsilon_{\beta\beta} & \gamma_{\beta z}\\ \gamma_{\alpha z} & \gamma_{\beta z} & \varepsilon_{zz}\end{array}\right]=\left[\begin{array}{ccc}\frac{\partial u_1}{\partial\alpha}+\frac{u_3}{R_\alpha} & \frac{\partial u_1}{\partial\beta}+\frac{\partial u_2}{\partial\alpha} & \frac{\partial u_1}{\partial z}+\frac{1}{a_1}\frac{\partial u_3}{\partial\alpha}-\frac{u}{R_\alpha}\\ \frac{\partial u_1}{\partial\beta}+\frac{\partial u_2}{\partial\alpha} & \frac{\partial u_2}{\partial\beta}+\frac{u_3}{R_\beta} & \frac{\partial u_2}{\partial z}+\frac{1}{a_2}\frac{\partial u_3}{\partial\beta}-\frac{v}{R_\beta}\\ \frac{\partial u_1}{\partial z}+\frac{1}{a_1}\frac{\partial u_3}{\partial\alpha}-\frac{u}{R_\alpha} & \frac{\partial u_2}{\partial z}+\frac{1}{a_2}\frac{\partial u_3}{\partial\beta}-\frac{v}{R_\beta} & 0\end{array}\right]\tag{4}$$

Herein, using the modified Sander's theory, the ultimate strain-displacement relations for a DCS can be written as (Kiani et al., 2013):

$$\left\{\begin{array}{c}\varepsilon_{\alpha\alpha}\\ \varepsilon_{\beta\beta}\\ \gamma_{\beta z}\\ \gamma_{\alpha z}\\ \gamma_{\alpha\beta}\end{array}\right\}=\left[\begin{array}{ccccc}\frac{\partial}{\partial\alpha} & 0 & \frac{1}{R_\alpha} & z\frac{\partial}{\partial\alpha} & 0\\ 0 & \frac{\partial}{\partial\beta} & \frac{1}{R_\beta} & 0 & z\frac{\partial}{\partial\beta}\\ 0 & -\frac{1}{R_\beta} & \frac{\partial}{\partial\beta} & 0 & 1\\ -\frac{1}{R_\alpha} & 0 & \frac{\partial}{\partial\alpha} & 1 & 0\\ (1+zC_0)\frac{\partial}{\partial\beta} & (1-zC_0)\frac{\partial}{\partial\alpha} & 0 & z\frac{\partial}{\partial\beta} & z\frac{\partial}{\partial\alpha}\end{array}\right]\left\{\begin{array}{c}u\\ v\\ w\\ \varphi_\alpha\\ \varphi_\beta\end{array}\right\}\tag{5}$$

where $C_0=\frac{1}{2}\left(\frac{1}{R_\alpha}-\frac{1}{R_\beta}\right)$.

Let us consider the linear relationship of strain gradient as (Malikan et al., 2023):

$$\eta_{ijk}=\frac{1}{2}\frac{\partial}{\partial x_k}\left(\frac{\partial u_i}{\partial x_j}+\frac{\partial u_j}{\partial x_i}\right)\tag{6}$$

The preceding magneto-elastic stress and hyperstress relations can be re-employed as (Malikan & Eremeyev, 2022c):

$$\sigma_{ij}=C_{ijkl}\varepsilon_{kl}-q_{ijk}H_k+r_{ijklm}\frac{\partial\varepsilon_{kl}}{\partial x_m}-h_{ijkl}\frac{\partial H_k}{\partial x_l}\tag{7}$$

$$\xi_{ijk}=g_{ijklmn}\frac{\partial\varepsilon_{lm}}{\partial x_n}+r_{ijklm}\varepsilon_{ij}-\lambda_{ijklm}\frac{\partial H_l}{\partial x_m}-f_{ijkl}H_l\tag{8}$$

$$T_{ij} = -b_{ijkl}\frac{\partial H_k}{\partial x_l} - s_{ijk}H_i - \lambda_{ijklm}\frac{\partial \varepsilon_{ij}}{\partial x_k} - h_{ijkl}\varepsilon_{ij} \tag{9}$$

$$B_i = a_{kl}H_k + q_{ijkl}\varepsilon_{ij} + s_{ijk}\frac{\partial H_j}{\partial x_k} + f_{ijkl}\frac{\partial \varepsilon_{ij}}{\partial x_k} \tag{10}$$

The variational relation is well-used and employed to establish accurate governing equations for thin-walled structures of any geometries. Let us proceed with the mathematical model based on this foundation.

$$\delta U - \delta W = 0 \tag{11}$$

Afterwards, one can expand Eq. (11) for the present model into two parts: the strain energy and, later, the works done by magnetic field.

$$\delta U = \int_0^a \int_0^b \int_{-h/2}^{h/2} \begin{bmatrix} \sigma_{\alpha\alpha}\delta\varepsilon_{\alpha\alpha} + \sigma_{\beta\beta}\delta\varepsilon_{\beta\beta} + \sigma_{\alpha\beta}\delta\varepsilon_{\alpha\beta} + \tau_{\alpha z}\delta\varepsilon_{\alpha z} + \tau_{\beta z}\delta\varepsilon_{\beta z} \\ +\xi_{\alpha\alpha z}\delta\eta_{\alpha\alpha z} + \xi_{\beta\beta z}\delta\eta_{\beta\beta z} + \xi_{\alpha\beta z}\delta\eta_{\alpha\beta z} + \xi_{\alpha\alpha\alpha}\delta\eta_{\alpha\alpha\alpha} \\ +\xi_{\alpha\alpha\beta}\delta\eta_{\alpha\alpha\beta} + \xi_{\beta\beta\beta}\delta\eta_{\beta\beta\beta} + \xi_{\beta\beta\alpha}\delta\eta_{\beta\beta\alpha} + \xi_{\alpha\beta\alpha}\delta\eta_{\alpha\beta\alpha} \\ +\xi_{\alpha\beta\beta}\delta\eta_{\alpha\beta\beta} + \xi_{\alpha z\alpha}\delta\eta_{\alpha z\alpha} + \xi_{\alpha z\beta}\delta\eta_{\alpha z\beta} + \xi_{\alpha zz}\delta\eta_{\alpha zz} \\ +\xi_{\beta z\alpha}\delta\eta_{\beta z\alpha} + \xi_{\beta z\beta}\delta\eta_{\beta z\beta} + \xi_{\beta zz}\delta\eta_{\beta zz} - T_{\alpha\alpha}\delta\dfrac{\partial H_\alpha}{\partial\alpha} \\ -T_{\beta\beta}\delta\dfrac{\partial H_\beta}{\partial\beta} - T_{zz}\delta\dfrac{\partial H_z}{\partial z} - B_\alpha\delta H_\alpha - B_\beta\delta H_\beta - B_z\delta H_z \end{bmatrix} a_1a_2a_3dzd\beta d\alpha \tag{12}$$

The external magnetic field impacts the energy of the domain, resulting in a thermodynamic work expressed as (Malikan & Nguyen, 2018):

$$\delta W = -\int_0^b \int_0^a \left\{ N^0_{\alpha\alpha}\left(\frac{\partial w}{\partial\alpha}\frac{\partial\delta w}{\partial\alpha}\right) + N^0_{\beta\beta}\left(\frac{\partial w}{\partial\beta}\frac{\partial\delta w}{\partial\beta}\right) + Q \right\} a_1a_2 d\alpha d\beta \tag{13}$$

Not to mention that the shear effect of the field is disregarded.

The matrix C_{ijkl} could be condensed to C_{ij} ($i, j \in \{1, 2, \ldots, 6\}$) utilizing the Voigt notation. The opportunity to decrease the elastic components arises when the structure demonstrates linear elastic behavior (Karami et al., 2019).

$$[C_{ijkl}] = \begin{bmatrix} C_{1111} & C_{1122} & C_{1133} & 0 & 0 \\ C_{1122} & C_{2222} & C_{2233} & 0 & 0 \\ C_{1133} & C_{2233} & C_{3333} & 0 & 0 \\ 0 & 0 & 0 & C_{1313} & 0 \\ 0 & 0 & 0 & 0 & C_{1212} \end{bmatrix} \tag{14}$$

where the stiffness matrix components for a *pure* elastic structure can be calculated by assuming isotropic plane strain as:

$$C_{1111} = \frac{E}{1-\nu^2}, C_{1122} = \frac{\nu E}{1-\nu^2}, C_{2222} = C_{1111}, C_{1313} = \frac{E}{1-\nu^2}\frac{1-\nu}{2},$$
$$C_{3333} = C_{1212} = C_{1313}, C_{1133} = C_{2233} = 0$$

In piezomagnetic materials with hexagonal crystalline structure, it is possible to simplify the piezomagnetic tensor as (Malikan et al., 2023):

$$[q_{ijk}] = \begin{bmatrix} 0 & 0 & 0 & 0 & q_{15} \\ 0 & 0 & 0 & q_{15} & 0 \\ q_{31} & q_{32} & q_{33} & 0 & 0 \end{bmatrix} \tag{15}$$

Similarly, the symmetry representations of the direct and reverse flexomagnetic parameters can be condensed into three independent elements, f_{11}, f_{111}, and f_{14} as applicable to a cubic crystal (Malikan et al., 2023).

$$[f_{ij}] = \begin{bmatrix} 0 & 0 & 0 & 0 & f_{111} \\ 0 & 0 & 0 & f_{111} & 0 \\ f_{14} & f_{14} & f_{11} & 0 & 0 \end{bmatrix} \tag{16}$$

Subsequently, due to insufficient literature on the same material, one may assume that the converse FM tensor aligns with the direct one, thereby allowing it to be reduced accordingly (considering the piezomagnetic material has been identified as a cubic crystal).

$$[h_{ij}] = \begin{bmatrix} 0 & 0 & 0 & 0 & h_{46} \\ 0 & 0 & 0 & h_{46} & 0 \\ h_{15} & h_{15} & h_{11} & 0 & 0 \end{bmatrix} \tag{17}$$

Designing empirically small-sized devices poses a challenge due to size dependence. Various micro-models can be employed to capture these small-scale characteristics (Malikan et l., 2019; Malikan & Sadraee Far, 2018; Malikan et al., 2020a; Dastjerdi et al., 2022; Stempin & Sumelka, 2022; Stempin et al., 2023; Dastjerdi & Akgöz, 2019; Dastjerdi et al., 2021b; Karami & Ghayesh, 2023; Barretta et al., 2023; Civalek et al., 2023). In this research, within the scheme of the strain gradient approach, the size effect is explored and utilized, and in consequence, the first Mindlin's model associated with isotropic and linear elastic materials can be (Sidhardh & Ray, 2018; Malikan & Eremeyev, 2022c; Malikan et al., 2023):

$$\begin{aligned} g_{ijklmn} &= g_1\left[\left(\delta_{ij}\delta_{kl}+\delta_{ik}\delta_{jl}\right)\delta_{mn}+\left(\delta_{im}\delta_{ln}+\delta_{in}\delta_{lm}\right)\delta_{jk}\right] \\ &+g_2\left[\delta_{ij}\left(\delta_{km}\delta_{ln}+\delta_{kn}\delta_{lm}\right)+\delta_{ik}\left(\delta_{jn}\delta_{lm}+\delta_{jm}\delta_{ln}\right)\right]+g_3\delta_{il}\delta_{jk}\delta_{mn} \\ &+g_4\delta_{il}\left(\delta_{jm}\delta_{kn}+\delta_{jn}\delta_{km}\right)+g_5\left[\delta_{im}\left(\delta_{jl}\delta_{kn}+\delta_{jn}\delta_{kl}\right)+\delta_{in}\left(\delta_{jl}\delta_{km}+\delta_{jm}\delta_{kl}\right)\right] \end{aligned} \tag{18}$$

It should be kept in mind that the material under scrutiny is a non-centrosymmetric piezomagnetic substance. However, the adoption of the centrosymmetric strain gradient tensor is a provisional assumption made due to a lack of ample literature. The elements of 'g' adhere to isotropic gradient elasticity.

It has already been recognized that

$$\delta_{\mathrm{ij}}=\begin{cases}1, if\,\mathrm{i}=\mathrm{j},\\ 0, if\,\mathrm{i}\neq\mathrm{j}.\end{cases} \tag{19}$$

Hence, for instance, one may articulate the first term of the strain gradient elastic moduli by applying the Voigt notation rules as follows:

$$g_{111111}=4(g_1+g_2+g_5)+g_3+2g_4 \tag{20}$$

The strain gradient parameters of the material can be formulated as follows (Sidhardh & Ray, 2018; Malikan & Eremeyev, 2022c; Malikan et al., 2023):

$$\begin{aligned} &g_1=-\frac{2}{3}(g_2+g_5),g_2=\frac{\mu}{30}\left(27l_0^2-4l_1^2-15l_2^2\right) \\ &g_3=\frac{1}{3}(8g_2+2g_5),g_4=\frac{\mu}{3}\left(l_1^2+6l_2^2\right),g_5=\frac{\mu}{3}\left(l_1^2-3l_2^2\right) \end{aligned} \tag{21}$$

where the introduced parameters l_0, l_1, and l_2 represent the material length scales.

To make things simpler, one may suppose that $l_0=l_1=l_2=l$ (Malikan et al., 2023). Besides, the precise value of the strain gradient shear modulus (μ) has not already been established. Therefore, its magnitude is treated as a scalar equivalent to the elastic shear modulus (G).

Numerous mathematical efforts are essential to derive the magnetic potential relationship, such as:

$$\begin{aligned} \Psi &= \left(\frac{h^2}{4}-z^2\right)\left[\frac{h_{46}}{2a_{33}}\left(\frac{\partial^3 u}{\partial\alpha^2\partial\beta}+\frac{\partial^3 v}{\partial\alpha^3}\right)+C_0\frac{zh_{46}}{6a_{33}}\left(\frac{\partial^3 u}{\partial\alpha^2\partial\beta}-\frac{\partial^3 v}{\partial\alpha^3}\right)+\frac{q_{31}}{2a_{33}}\frac{\partial\varphi_\alpha}{\partial\alpha}\right. \\ &\left.+\frac{zh_{46}}{6a_{33}}\left(\frac{\partial^3\varphi_\beta}{\partial\alpha^3}+\frac{\partial^3\varphi_\alpha}{\partial\alpha^2\partial\beta}\right)+\frac{q_{32}}{2a_{33}}\frac{\partial\varphi_\beta}{\partial\beta}+\frac{h_{46}}{2a_{33}}\left(\frac{\partial^2\varphi_\alpha}{\partial\beta^2}+\frac{\partial^3 w}{\partial\alpha\partial\beta^2}-\frac{1}{R_\alpha}\frac{\partial^2 u}{\partial\beta^2}\right)\right]+\psi\left(\frac{1}{2}+\frac{z}{h}\right) \end{aligned} \tag{22}$$

The following conditions have been presumed for the magnetic potential through the thickness of the media that can be satisfied by Eq. (22).

$$\Psi\left(+\frac{h}{2}\right)=\psi,\Psi\left(-\frac{h}{2}\right)=0 \tag{23}$$

Let us gather the terms in Eqs. (12) and (13) that pertain to the governing equations. Then, a substantial amount of mathematical processing gives

$$\begin{aligned} &\frac{\partial N_{\alpha\alpha}}{\partial\alpha}+\frac{\partial N_{\alpha\beta}}{\partial\beta}+\frac{\partial^2 T_{\alpha\alpha\alpha}}{\partial\alpha^2}+\frac{\partial^2 T_{\alpha\beta\beta}}{\partial\beta^2}+\frac{\partial^2}{\partial\alpha\partial\beta}\left(T_{\alpha\alpha\beta}+T_{\alpha\beta\alpha}\right)-\frac{1}{R_\alpha}\left(\frac{\partial T_{\alpha z\alpha}}{\partial\alpha}+\frac{\partial T_{\alpha z\beta}}{\partial\beta}-Q_{\alpha z}\right) \\ &+C_0\left[\frac{\partial}{\partial\beta}\left(M_{\alpha\beta}+T_{\alpha\beta z}\right)+\frac{\partial^2 R_{\alpha\beta\alpha}}{\partial\alpha\partial\beta}+\frac{\partial^2 R_{\alpha\beta\beta}}{\partial\beta^2}\right]=0 \end{aligned} \tag{24a}$$

$$\begin{aligned} &\frac{\partial N_{\alpha\beta}}{\partial\alpha}+\frac{\partial N_{\beta\beta}}{\partial\beta}+\frac{\partial^2 T_{\alpha\beta\alpha}}{\partial\alpha^2}+\frac{\partial^2 T_{\beta\beta\beta}}{\partial\beta^2}+\frac{\partial^2}{\partial\alpha\partial\beta}\left(T_{\beta\beta\alpha}+T_{\alpha\beta\beta}\right)-\frac{1}{R_\beta}\left(\frac{\partial T_{\beta z\alpha}}{\partial\alpha}+\frac{\partial T_{\beta z\beta}}{\partial\beta}-Q_{\beta z}\right) \\ &-C_0\left[\frac{\partial}{\partial\alpha}\left(M_{\alpha\beta}+T_{\alpha\beta z}\right)+\frac{\partial^2 R_{\alpha\beta\alpha}}{\partial\alpha^2}+\frac{\partial^2 R_{\alpha\beta\beta}}{\partial\alpha\partial\beta}\right]=0 \end{aligned} \tag{24b}$$

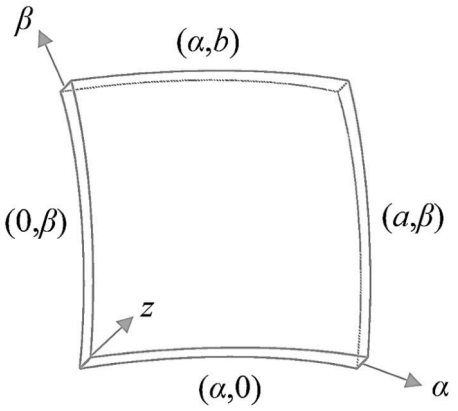

Fig. 2. Coordinates for edges.

$$\frac{\partial Q_{\alpha z}}{\partial \alpha}+\frac{\partial Q_{\beta z}}{\partial \beta}+\frac{1}{R_\alpha}\left(\frac{\partial T_{\alpha\alpha\alpha}}{\partial \alpha}+\frac{\partial T_{\alpha\alpha\beta}}{\partial \beta}-N_{\alpha\alpha}\right)+\frac{1}{R_\beta}\left(\frac{\partial T_{\beta\beta\beta}}{\partial \beta}+\frac{\partial T_{\beta\beta\alpha}}{\partial \alpha}-N_{\beta\beta}\right)+\frac{\partial^2 T_{\alpha z\alpha}}{\partial \alpha^2}$$
$$+\frac{\partial^2 T_{\beta z\beta}}{\partial \beta^2}+\frac{\partial^2}{\partial \alpha\partial \beta}\left(T_{\alpha z\beta}+T_{\beta z\alpha}\right)+N^0_{\alpha\alpha}\frac{\partial^2 w}{\partial \alpha^2}+N^0_{\beta\beta}\frac{\partial^2 w}{\partial \beta^2}=Q \tag{24c}$$

$$\frac{\partial M_{\alpha\alpha}}{\partial \alpha}+\frac{\partial M_{\alpha\beta}}{\partial \beta}+\frac{\partial}{\partial \alpha}\left(T_{\alpha\alpha z}+T_{\alpha z\alpha}\right)+\frac{\partial}{\partial \beta}\left(T_{\alpha z\beta}+T_{\alpha\beta z}\right)+\frac{\partial^2}{\partial \alpha\partial \beta}\left(R_{\alpha\alpha\beta}+R_{\alpha\beta\alpha}\right)$$
$$+\frac{\partial^2 R_{\alpha\alpha\alpha}}{\partial \alpha^2}+\frac{\partial^2 R_{\alpha\beta\beta}}{\partial \beta^2}-Q_{\alpha z}=0 \tag{24d}$$

$$\frac{\partial M_{\alpha\beta}}{\partial \alpha}+\frac{\partial M_{\beta\beta}}{\partial \beta}+\frac{\partial}{\partial \alpha}\left(T_{\beta z\alpha}+T_{\alpha\beta z}\right)+\frac{\partial}{\partial \beta}\left(T_{\beta\beta z}+T_{\beta z\beta}\right)+\frac{\partial^2}{\partial \alpha\partial \beta}\left(R_{\alpha\beta\beta}+R_{\beta\beta\alpha}\right)$$
$$+\frac{\partial^2 R_{\alpha\beta\alpha}}{\partial \alpha^2}+\frac{\partial^2 R_{\beta\beta\beta}}{\partial \beta^2}-Q_{\beta z}=0 \tag{24e}$$

Eq. (24) can serve as a reference point for governing equations of smart doubly-curved shells. The aforesaid lower-order internal forces of the PFMDCSs can be signified as follows:

$$\begin{bmatrix} N_{\alpha\alpha} & M_{\alpha\alpha} \\ N_{\beta\beta} & M_{\beta\beta} \\ N_{\alpha\beta} & M_{\alpha\beta} \end{bmatrix}=\int_{-h/2}^{h/2}\begin{Bmatrix} \sigma_{\alpha\alpha} \\ \sigma_{\beta\beta} \\ \tau_{\alpha\beta} \end{Bmatrix}(1,z)dz \tag{25a}$$

$$\left\{Q_{\alpha z},Q_{\beta z}\right\}=k_s\int_{-h/2}^{h/2}\left\{\tau_{\alpha z},\tau_{\beta z}\right\}dz \tag{25b}$$

$$\left\{N^0_{\alpha\alpha},N^0_{\beta\beta}\right\}=-\frac{\psi}{h}\int_{-h/2}^{h/2}q_{31}dz \tag{25c}$$

where the correction factor for the transverse shear stresses could be taken as the classic value k_s=5/6.

And the higher-order internal forces that belong to the strain gradients are:

$$\begin{bmatrix} T_{\alpha\alpha\alpha} & T_{\alpha\alpha\beta} & T_{\alpha\alpha z} \\ T_{\beta\beta\alpha} & T_{\beta\beta\beta} & T_{\beta\beta z} \\ T_{\alpha z\alpha} & T_{\alpha z\beta} & T_{\alpha zz} \\ T_{\beta z\alpha} & T_{\beta z\beta} & T_{\beta zz} \\ T_{\alpha\beta\alpha} & T_{\alpha\beta\beta} & T_{\alpha\beta z} \end{bmatrix}=\int_{-h/2}^{h/2}\begin{bmatrix} \xi_{\alpha\alpha\alpha} & \xi_{\alpha\alpha\beta} & \xi_{\alpha\alpha z} \\ \xi_{\beta\beta\alpha} & \xi_{\beta\beta\beta} & \xi_{\beta\beta z} \\ \xi_{\alpha z\alpha} & \xi_{\alpha z\beta} & \xi_{\alpha zz} \\ \xi_{\beta z\alpha} & \xi_{\beta z\beta} & \xi_{\beta zz} \\ \xi_{\alpha\beta\alpha} & \xi_{\alpha\beta\beta} & \xi_{\alpha\beta z} \end{bmatrix}dz \tag{26}$$

Following that, the higher-order moment resultants can also be revealed as:

$$\begin{bmatrix} R_{\alpha\alpha\alpha} & R_{\alpha\alpha\beta} & R_{\alpha\alpha z} \\ R_{\beta\beta\alpha} & R_{\beta\beta\beta} & R_{\beta\beta z} \\ R_{\alpha z\alpha} & R_{\alpha z\beta} & R_{\alpha zz} \\ R_{\beta z\alpha} & R_{\beta z\beta} & R_{\beta zz} \\ R_{\alpha\beta\alpha} & R_{\alpha\beta\beta} & R_{\alpha\beta z} \end{bmatrix} = \int_{-h/2}^{h/2} \begin{bmatrix} \xi_{\alpha\alpha\alpha} & \xi_{\alpha\alpha\beta} & \xi_{\alpha\alpha z} \\ \xi_{\beta\beta\alpha} & \xi_{\beta\beta\beta} & \xi_{\beta\beta z} \\ \xi_{\alpha z\alpha} & \xi_{\alpha z\beta} & \xi_{\alpha zz} \\ \xi_{\beta z\alpha} & \xi_{\beta z\beta} & \xi_{\beta zz} \\ \xi_{\alpha\beta\alpha} & \xi_{\alpha\beta\beta} & \xi_{\alpha\beta z} \end{bmatrix} z dz \tag{27}$$

3. Space solution

If one solves Eq. (24), the numerical values for deflections will be provided for the PFM nanocomposite shell-like structures. A straightforward analytical process is complemented in this section. The process is conducted under immovable simple edge conditions grounded in double-series concepts, where the edge coordinates can be diagnosed by Fig. 2.

Accordingly, the executed conditions for force and geometrical boundaries can be illustrated as:

$$u(\alpha,0) = u(\alpha,b) = u(0,\beta) = u(a,\beta) = 0 \tag{28a}$$

$$v(\alpha,0) = v(\alpha,b) = v(0,\beta) = v(a,\beta) = 0 \tag{28b}$$

$$w(\alpha,0) = w(\alpha,b) = w(0,\beta) = w(a,\beta) = 0 \tag{28c}$$

$$\varphi_\alpha(\alpha,0) = \varphi_\alpha(\alpha,b) = 0, \varphi_\beta(0,\beta) = \varphi_\beta(a,\beta) = 0 \tag{28d}$$

$$M_{\alpha\alpha}(0,\beta) = M_{\alpha\alpha}(a,\beta) = 0, M_{\beta\beta}(\alpha,0) = M_{\beta\beta}(\alpha,b) = 0 \tag{28e}$$

To implement the analytical solution, the double-series functions can be deployed as (Dindarloo et al., 2020)

$$\begin{Bmatrix} u \\ v \\ w \\ \varphi_\alpha \\ \varphi_\beta \end{Bmatrix} = \sum_{m=1}^{\infty}\sum_{n=1}^{\infty} \begin{Bmatrix} U_{mn}\cos\left(\frac{m\pi}{a}\alpha\right)\sin\left(\frac{n\pi}{b}\beta\right) \\ V_{mn}\sin\left(\frac{m\pi}{a}\alpha\right)\cos\left(\frac{n\pi}{b}\beta\right) \\ W_{mn}\sin\left(\frac{m\pi}{a}\alpha\right)\sin\left(\frac{n\pi}{b}\beta\right) \\ \Phi_{\alpha mn}\cos\left(\frac{m\pi}{a}\alpha\right)\sin\left(\frac{n\pi}{b}\beta\right) \\ \Phi_{\beta mn}\sin\left(\frac{m\pi}{a}\alpha\right)\cos\left(\frac{n\pi}{b}\beta\right) \end{Bmatrix} \tag{29}$$

where the Fourier series dedicated to each unknown variable becomes a solution to the bending constitutive equations.

The system of algebraic equations can be determined by replacing Eq. (29) into the bending equations and then summarily shown as:

$$\left[K_{ij}\right]_{5\times5}\{\Delta_{mn}\}_{5\times1} = \{Q_{mn}\}_{5\times1} \tag{30}$$

in which K is the stiffness matrix whose overall coefficients are independent to the bending load. The unknown vector can be described as:

$$\Delta_{mn} = \left(U_{mn}, V_{mn}, W_{mn}, \Phi_{\alpha mn}, \Phi_{\beta mn}\right)^T \tag{31}$$

$$Q_{mn} = (0,0,Q,0,0)^T \tag{32}$$

The force that is uniform and applied constantly and vertically on the shell top surface ($+h/2$) can be expressed as (Wang et al., 2018):

$$Q = \sum_{m=1}^{\infty}\sum_{n=1}^{\infty} Q_0 \sin\left(\frac{m\pi}{a}\alpha\right)\sin\left(\frac{n\pi}{b}\beta\right) \tag{33}$$

where $Q_0 = \frac{16q_0}{mn\pi^2}$ is defined for a constant uniform transverse load per area.

Computing the variables of Eq. (31) by Eq. (30) provides the amounts of small deflections for PFMDCSs. To undertake this, the Newton-Raphson algorithm can reach out to deliver the results (Dastjerdi & Jabbarzadeh, 2016):

$$\begin{Bmatrix} U_{mn,p+1} \\ V_{mn,p+1} \\ W_{mn,p+1} \\ \Phi_{\alpha mn,p+1} \\ \Phi_{\beta mn,p+1} \end{Bmatrix} = \begin{Bmatrix} U_{mn,p} \\ V_{mn,p} \\ W_{mn,p} \\ \Phi_{\alpha mn,p} \\ \Phi_{\beta mn,p} \end{Bmatrix} - J^{-1} \times A_p \tag{34}$$

Table 1
Different geometries for revoluted doubly-curved shell-like structures.

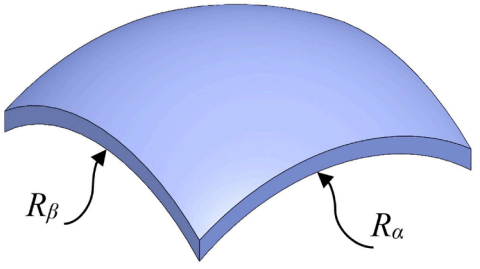

Spherical Geometry (SG): $R_\alpha = R_\beta = R$

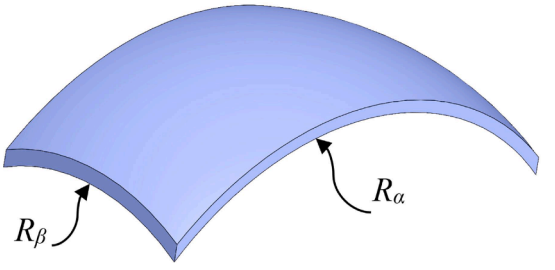

Elliptical Geometry (EG): $R_\beta = R, R_\alpha = 2R$

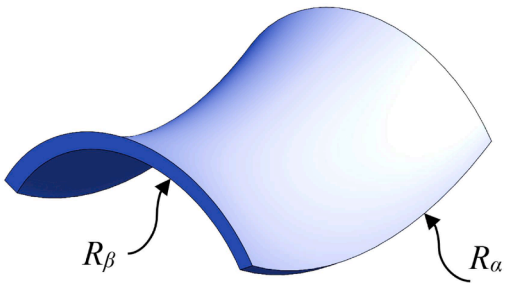

Hyperbolic Geometry (HG): $R_\beta = R, R_\alpha = -R$

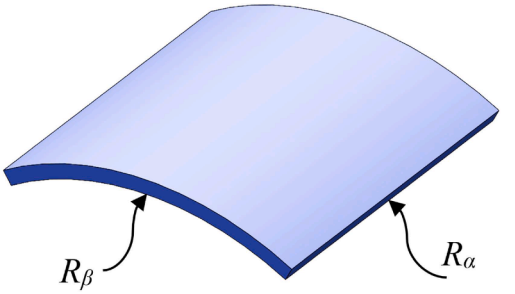

Cylindrical Geometry (CG): $R_\beta = R, R_\alpha = \infty$

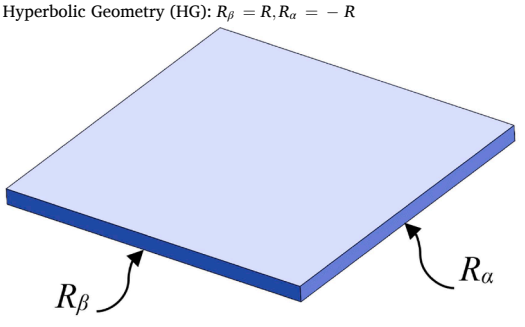

Plate Geometry (PG): $R_\alpha = R_\beta = \infty$

*The 3D models were drawn in SolidWorks 2023 for non-commercial research and instructional purposes.
*All the designed shapes are shells of revolution.
*According to the chord calculations for circular shells and in order to have circular DCSs, then a, b≤2R.

where

$$A_p = e\left\{U_{mn,p}, V_{mn,p}, W_{mn,p}, \Phi_{\alpha mn,p}, \Phi_{\beta mn,p}\right\}^{-1} \tag{35}$$

The primary guess $\{U_{mn,0}, V_{mn,0}, W_{mn,0}, \Phi_{\alpha mn,0}, \Phi_{\beta mn,0}\}$ plays the dominant role of a quicker convergence under lower iterations (p). Moreover, e denotes the governing equations (Eq. 24). Further, the Jacobian matrix can be formulated as:

$$J = \frac{\partial A_p}{\partial u_i}; u_i = \left\{U_{mn}, V_{mn}, W_{mn}, \Phi_{\alpha mn}, \Phi_{\beta mn}\right\}^{-1} \tag{36}$$

Lastly, the computer code will be implemented in MATLAB software.

4. Validation with FEM

The established shell model is generic in nature. Hence, one can develop it towards several other configurations notified and visualized in Table 1 (Mehar et al., 2021).

The precision and reliability of the proposed models in Table 1 can be identified through finite element commercial codes if one simplifies it by abandoning the PFM properties. This case is addressed through Fig. 3. To verify the reduced model, Abaqus simulation results are carried out for a linear static bending of shells subject to a lateral uniform load supplemented in simple boundary supports,

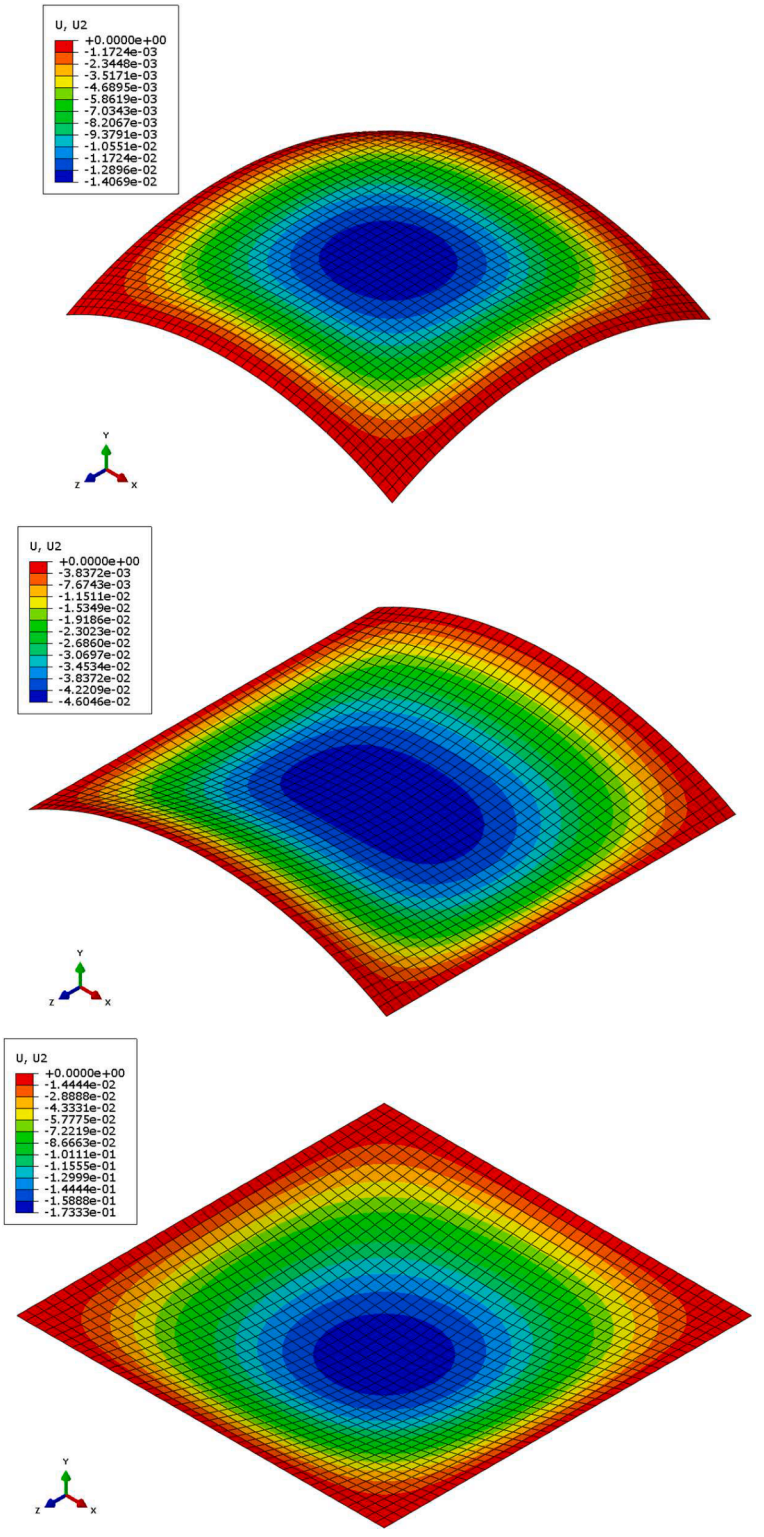

Fig. 3. a. Validation of non-smart doubly-curved shells with Abaqus/CAE, 3b. Validation of non-smart cylindrical shells with Abaqus/CAE, 3c. Validation of non-smart plates with Abaqus/CAE.

Table 2
Validation of doubly-curved shells with FEM results.

q_0 (MPa)	Maximum transverse deflection (mm) Analytical model $\times 10^{-2}$	Abaqus $\times 10^{-2}$	Discrepancy (%)
1	1.4349	1.4069	1.9901
2	2.8698	2.8137	1.9938
3	4.3047	4.2206	1.9926
4	5.7397	5.6274	1.9955
5	7.1746	7.0343	1.9945

Table 3
Validation of cylindrical shells with FEM results.

q_0 (MPa)	Maximum transverse deflection (mm) Analytical model $\times 10^{-2}$	Abaqus $\times 10^{-2}$	Discrepancy (%)
1	4.7020	4.6046	2.1152
2	9.4041	9.2092	2.1163
3	14.1062	13.8138	2.1167
4	18.8083	18.4184	2.1169
5	23.5104	23.0230	2.1170

Table 4
Validation of plates with FEM results.

q_0 (MPa)	Maximum transverse deflection (mm) Analytical model	Abaqus	Discrepancy (%)
1	0.1776	0.1733	2.4812
2	0.3553	0.3466	2.5100
3	0.5330	0.5199	2.5197
4	0.7107	0.6932	2.5245
5	0.8884	0.8665	2.5274

and the variables $R = a = b = 100$ mm, $h = 5$ mm, $E = 210$ GPa, ν=0.28 are utilized. It is to be noted that, in Abaqus, the nonlinear effect option has been deactivated and a linear 2D shell element has been used. What is more, it is noteworthy that the value of transverse pressure is affected by the curvature of the shells in the FEM software. In addition, the values of the lateral load have been chosen in such a manner that the deflections are retained as small as possible. Furthermore, for the Newton-Raphson program, a few iterations are adequate to reach convergence and terminate the loop.

By illustrating Tables 2,3,4, a good agreement is shown. In consequence, the capability of the present shell model and the used solution process can be verified. Thereupon, let us return to the main goal of this study and conduct the results for smart DCSs by dint of a parametric perusal in the succeeding section.

5. Results and discussions

In what follows, the results will belong to $CoFe_2O_4$ piezoceramic material to shift them to the engineering point of view (Zhou et al., 2012). What is more, all the bending results are held for the first mode number only.

Let us introduce some dimensionless ratios to build the numerical outcomes use-wider, $w* = W/h, l* = l/h, b* = b/h, R* = R/h, S* = a/b, \psi* = \psi f_{14}/abq_0, q_0* = 1/\psi*$.

The process goes on with the modal analysis and the illustration of the first eight mode shapes of the shells with the aid of Figs. 4,5,6,7,8. These normalized mode shapes are developed for simply-supported edge conditions only, and as far as the author is aware, are produced for the first time for square SG, HG, EG, and CG thin shells. The eigenmodes of a square PG shell with the same conditions have already been displayed (Karami & Ghayesh, 2024). As noticed by figures, axial half-wave numbers m and n are crystally clear, for example for SG and 2nd mode number, one finds $m = 2$, $n = 1$.

5.1. Influence of aspect ratio

The dimensionless ratio of the length to width, or aspect ratio (S) is one of the most vital parameters discussed in the mechanical analysis of shells and plates. To check this parameter for the types of shells shown in Table 1, Fig. 9 has been drawn. Considering that the relations have been calculated for linear bending, it is tried to keep all the deflections in this figure and beyond within the range of small deflections. In addition, the ratio of the length and width of the shell to the radius has been put within the allowed geometric range, which is defined in Table 1. It should be remembered that the figures included results for smart and non-smart shells, that means the non-smart shells have the full properties of PFM also strain gradient value but are not supposed to be magnetized and do not react

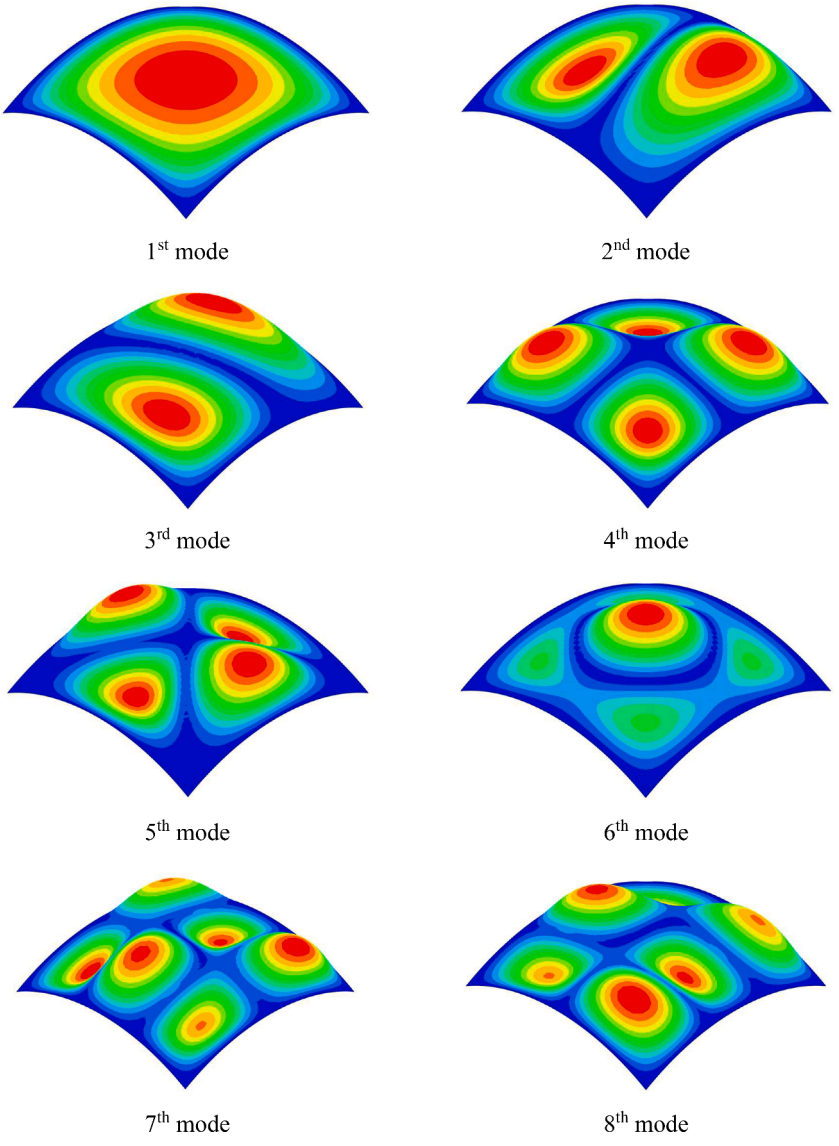

Fig. 4. Presentation of eigenmodes for SG.

to the magnetic environment. According to the results of this figure, the increase in the ratio of the length to the width of the shells leads to raising the stiffness of the shells, which actually means that the increase in the ratio of length to width results in a decrease in the elastic strength of the structures. However, this process is not the same for all the defined geometries. In hyperbolic geometry, first, a rise in the deflection is seen, but after a certain value of the S coefficient, a diminishment in the deflections is witnessed in this type of shell. In fact, this issue can be due to the inverse radius in the α dimension, which, with increasing length, leads to more stiffness and strength of the shells.

On the other hand, an invaluable result that can be extracted from this figure is that the difference in results between smart and non-smart DCSs is not the same for all types. The biggest difference in the cylindrical shell and the smallest difference in the hyperbolic shell and plate geometry can be observed. This result can express the theory that the electro-magnetic response of structures strongly depends on their geometry. However, this new result needs to be further evaluated under different conditions in the following figures so that it can be stated with certainty. In addition to this, smart DCSs display further strength in contrast to non-smart ones.

And at last, when the different geometries of double shells are examined, it is clear that the most resistant and stiffest are respectively spherical, elliptical, cylindrical, plate-shaped, and hyperbolic DCSs which has also been captured earlier by some other researchers (Wang et al., 2018). This means that DCSs are much stiffer than plates and can be highly efficient engineered structures. It should be pointed out that this result is not general and is contingent on several mechanisms such as boundary conditions, outer forces, material isotropy, and problem circumstances etc., and other analyses may probably deny such a conclusion.

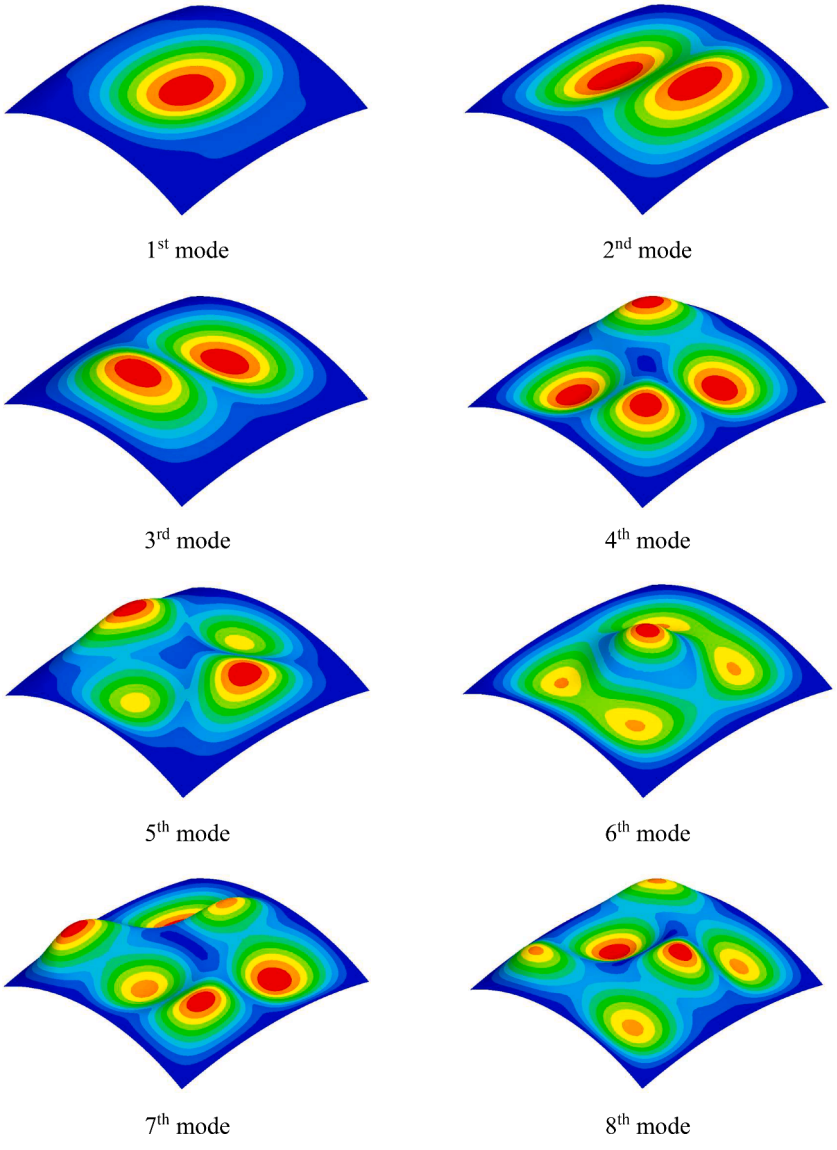

Fig. 5. Presentation of eigenmodes for EG.

5.2. *Strain gradient effect*

Since the discussion of this study is about the higher-order effects of magnetism, which are usually less studied, such as flexomagnetism, so then it is crucial to focus specifically on the impacts of the strain gradient. Because strain gradient generates flexomagnetic effect or flexoelectricity in smart materials. Inside the crystal of the ceramic material, the axial strain gradient helps to move the central ions so that this process leads to polarization inside the crystal. According to Fig. 10, it signifies the length scale variable in different values greatly affects the mechanical behavior of shells. Such an effect results in an increase in the mechanical strength and stiffness of structures. However, this effect is not the same in different geometries, and for example, the greatest effect in the hyperbolic shell can be depicted. In addition, the result obtained in the previous figure is confirmed here. It can be seen that the difference between smart and non-smart DCSs is not the same and in some shells, there is a bigger difference. Therefore, one can say that the electromagnetic response of structures is firmly contingent on their geometry and the geometry of the shell determines the amount of its intelligent response.

5.3. *Radius effect*

The effect of the size and magnitude of the DCSs radius on its electro-magneto-mechanical behavior is evaluated and studied by presenting Fig. 11. The size of the radius has been set in a defined range to come by the results. It is clear from these results that as the

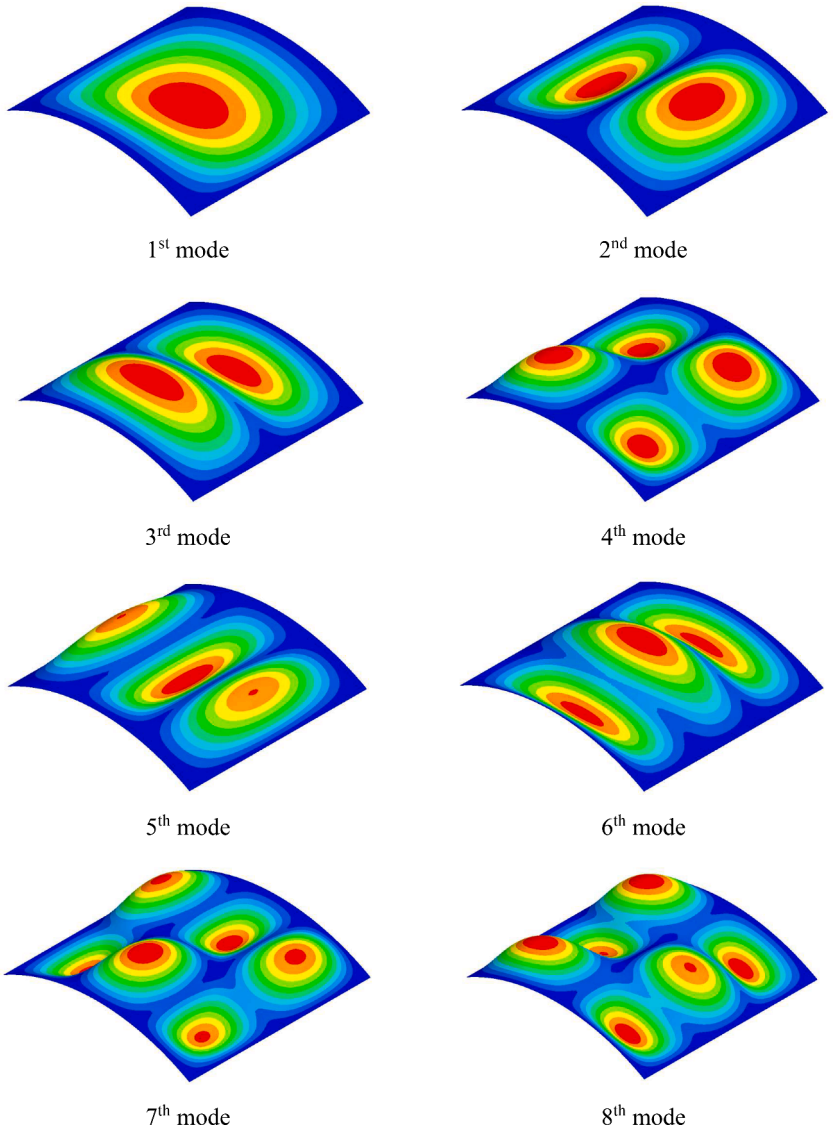

Fig. 6. Presentation of eigenmodes for CG.

size of the radius increases, the static deflection values also become greater. Nevertheless, this process is not true for the hyperbolic shell, and it is even the opposite. In general, hyperbolic shallow shells show a different mechanical behavior than the rest of the shells due to the fact that one of their radii is in an inverted form. Therefore, these types of shells cannot be suitable for engineering structures where high stability of the shell is required. Of course, this result is confirmed for the cases studied here only, and it may not be the case in other situations. In the continuation of scrutiny from this figure, it can be demonstrated that changes in the radius do not affect the results of the plate, which is completely logical because the plates are the same as DCSs but with an infinite radius, and the change in infinity is mathematically meaningless.

5.4. Effect of lateral load

Since the problem under study is the static bending of shells, it is important to know what effect different amounts of transverse load encounter on the mechanical behavior of these engineering structures. The analysis is started with a zero value for lateral load, i.e., the shells without transverse static force but in the electro-magnetic environment. The high transverse load leads to very large deflections, and this is not desirable because the goal is to keep the values of the deflections in the range of small deflections, which, according to the references small deflections values are usually between ten and fifteen percent of the thickness of the structure (Malikan & Eremeyev, 2020c). So the load has been considered as low as possible. The very interesting point in Fig. 12 is that when there is no lateral force on the shells, very small displacements occur, which is the result of the electro-magnetic field. These very small

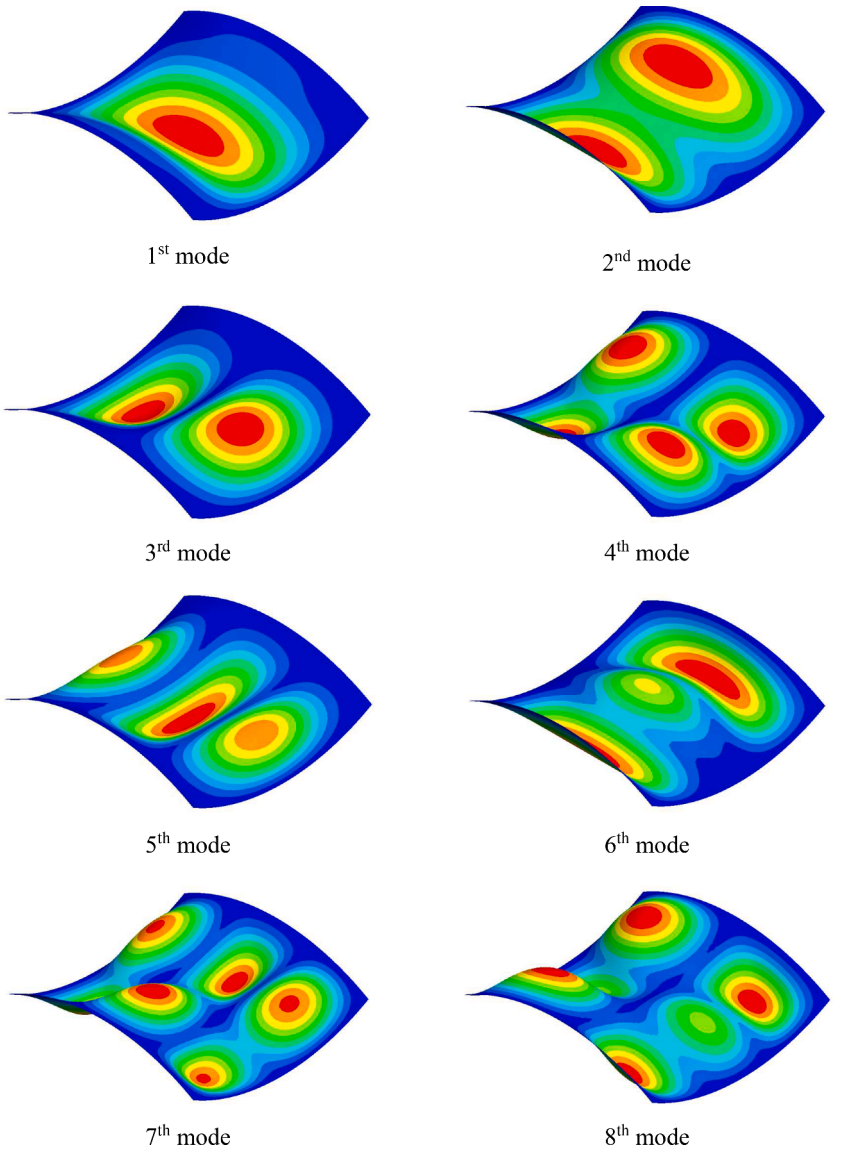

Fig. 7. Presentation of eigenmodes for HG.

deflection values are close to zero in the hyperbolic shell and the plate, but they are not equal to zero and are a little more noticeable in other shells. Of course, it goes without saying that the values of deflections without a static load fully depend on the value of the magnetic potential, and if the value of this parameter is chosen larger, these very small displacements can become more remarkable. However, this point is of great importance because the selection of large values for the magnetic potential itself leads to a significant reduction of the displacements and makes it difficult to distinguish between the deflections of different shells. This matter will be examined in the next figure. To end the review of the present figure, it is vividly exhibited that the large amounts of lateral force bring about more difference among the responses of all types of shells.

5.5. Influence of magnetic field

Fig. 13 will expand the current discussion by studying the effect of changes in magnetic potential on the electro-magnetic behavior of shells. First of all, it must be mentioned that the changes in the value of the magnetic potential do not affect the mechanical response of non-smart shells because their electro-magnetic properties are dismissed. References (Malikan & Eremeyev, 2020c) have completely shown that larger values of the magnetic potential cause greater stiffness of the internal structure of the material, which is caused by the greater contraction of the internal microstructure due to the magnetic environment. Consequently, there is a corresponding decrease in deflection value with an increase in magnetic potential value. Of course, the declining trend of the deflection in the spherical, elliptical, and cylindrical geometries is greater than in the hyperbolic and flat plate geometries. This is reminiscent of the

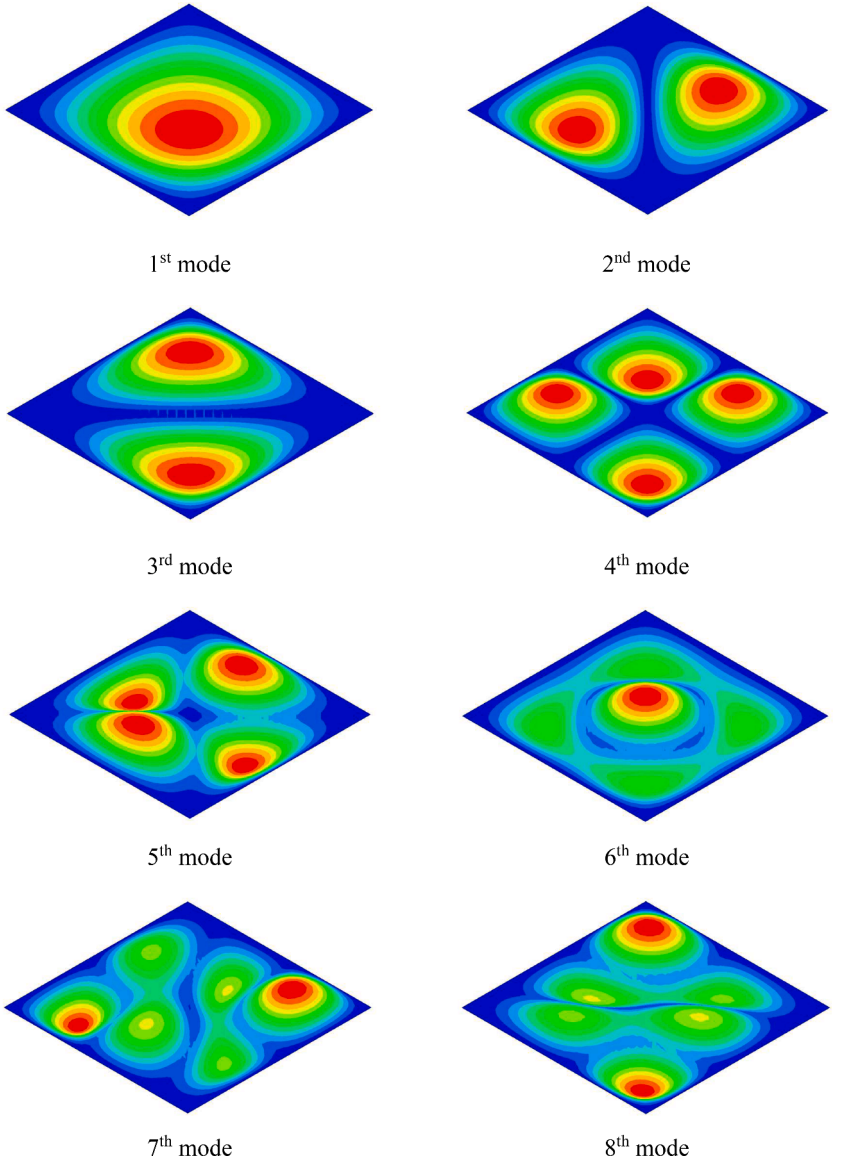

Fig. 8. Presentation of eigenmodes for PG.

valuable result achieved in the previous figures: that there is a strong linkage between the type of geometry and the magnetic field impact.

6. Conclusions

Smart shell models have been developed composed of lower- as well as higher-order magnetic influences. This model extends the existing literature on shell studies. To figure this out, the modified Sander's theory has been operated on to be basis of the mathematical model. The novel constitutive equations governing the intelligent doubly-curved shell structures have been attained based on a variationally consistent derivation process. The Navier-type exact solutions have completed the task of generating numerical results. To determine the validity and correctness of the mathematical model and the solution procedure, a streamlined FEM model that neglected the smart effects has been built by means of commercially predefined tools. A featured and elemental parametric study has been put into this work. Generally, some points have been gained through the case study, which are itemized below:

- Doubly-curved shallow shells with a spherical revolution can be coherently a high-strength engineering structure compared to flat plates.
- The spherical type of DCSs indicates further material stiffness in comparison with the rest of the types.
- In smart DCSs under bending forces, even if the shell is unloaded from lateral forces, the electro-magnetic field can cause very

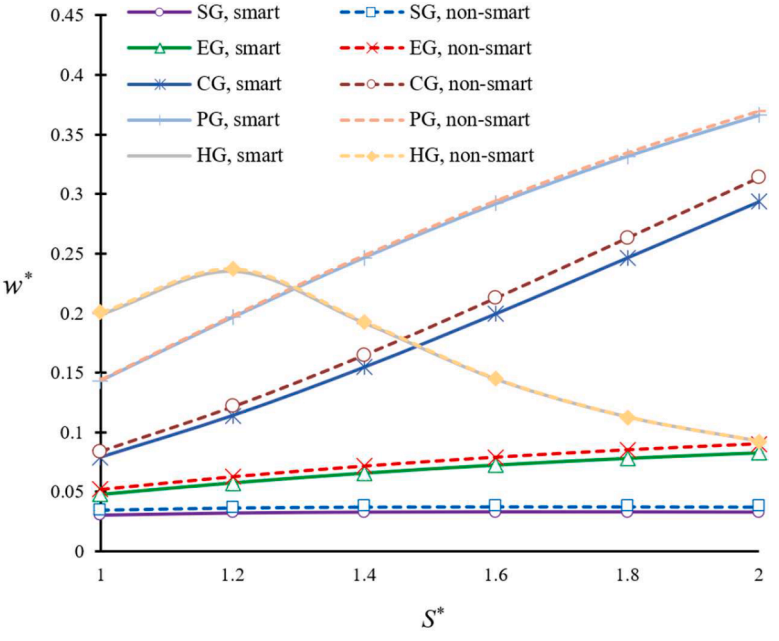

Fig. 9. Deflections vs. aspect ratio (l^*=0.2, b^*=20, R^*=b, $q_0{}^*$=1e6).

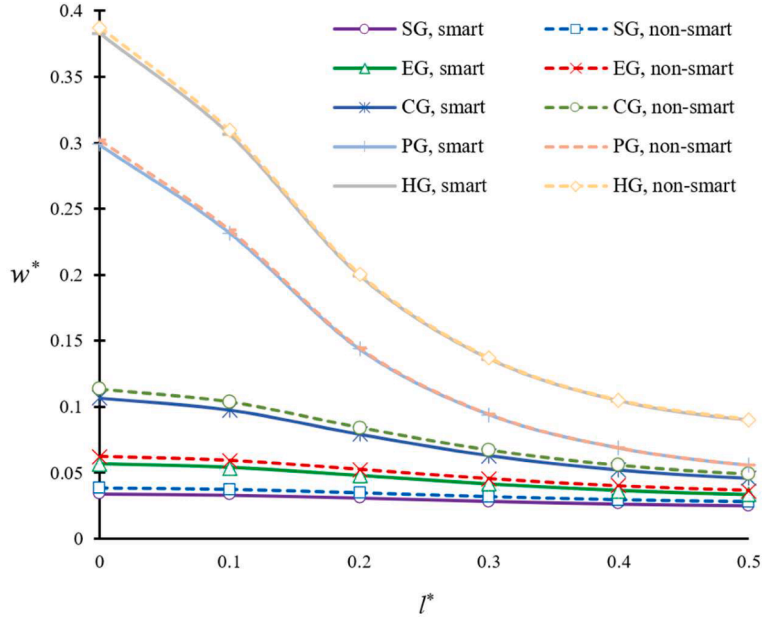

Fig. 10. Deflections vs. strain gradient ratio (b^*=20, R^*=b^*, S^*=1, $q_0{}^*$=1e6).

small static deflections.

- It has been concluded that the smart response and behavior of electro-magnetic structures can be straightforwardly related to their kind of geometry.

It should be brought to attention that current results can be extended to piezoelectric shell structures comprising flexoelectricity (Eremeyev et al., 2020; Mawassy et al., 2021; Malikan & Eremeyev, 2020d; Guinovart-Sanjuán et al., 2023) that is a similar phenomenon.

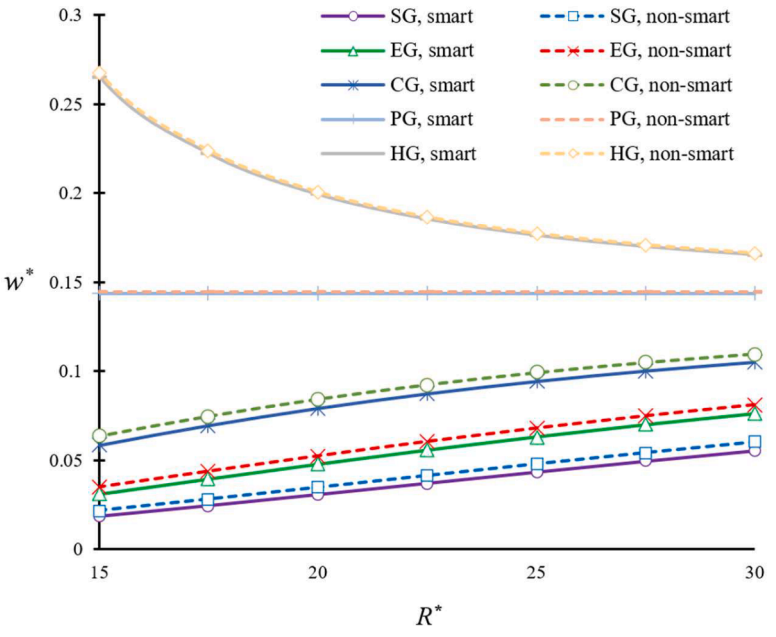

Fig. 11. Deflections vs. radius ratio (b^*=20, S^*=1, l^*=0.2, $q_0{}^*$=1e6).

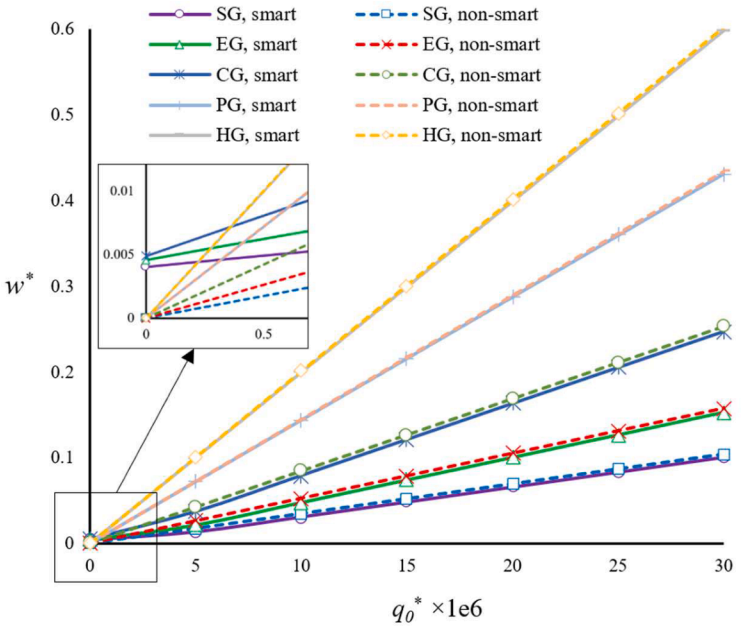

Fig. 12. Deflections vs. lateral load (b^*=20, S^*=1, R^*=b^*, l^*=0.2).

CRediT authorship contribution statement

Mohammad Malikan: Conceptualization, Methodology, Data curation, Writing – original draft, Writing – review & editing, Visualization, Software, Validation, Formal analysis, Resources, Investigation, Project administration, Supervision, Funding acquisition.

Declaration of competing interest

There are no competing interests to declare.

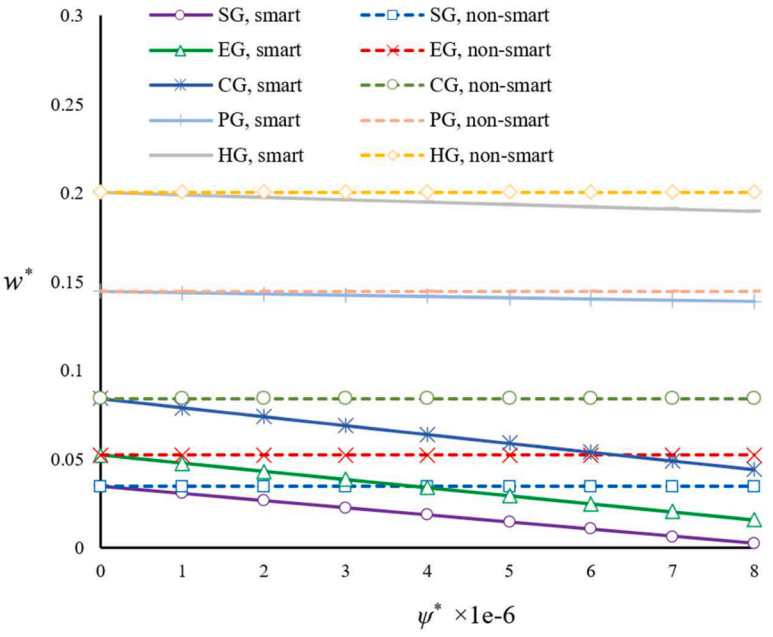

Fig. 13. Deflections vs. magnetic field (b^*=20, S^*=1, R^*=b^*, l^*=0.2, $q_0{}^*$=1e6).

Data availability

The data is a part of future research and cannot be shared.

Acknowledgements

The studies on the piezocomposites is a part of the grant ARGENTUM TRIGGERING RESEARCH GRANTS - 'Excellence Initiative - Research University' (Project no. 9/1/2022/IDUB/I3b/Ag) which was financially supported by Gdańsk University of Technology, Gdańsk, Poland.

Computations were carried out using the computers of Center of Informatics Tricity Academic Supercomputer & Network (TASK). The full licensed versions of software packages have been supplied from TASK center.

References

Ahmadi, H., Bayat, A., & Duc, N. D. (2021). Nonlinear forced vibrations analysis of imperfect stiffened FG doubly curved shallow shell in thermal environment using multiple scales method. *Composite Structures, 256*, Article 113090.

Alijani, F., Amabili, M., Karagiozis, K., & Bakhtiari-Nejad, F. (2011). Nonlinear vibrations of functionally graded doubly curved shallow shells. *Journal of Sound and Vibration, 330*, 1432–1454.

Amabili, M. (2005). Non-linear vibrations of doubly curved shallow shells. *International Journal of Non-Linear Mechanics, 40*, 683–710.

Amabili, M., & Reddy, J. N. (2010). A new non-linear higher-order shear deformation theory for large-amplitude vibrations of laminated doubly curved shells. *International Journal of Non-Linear Mechanics, 45*, 409–418.

Aminipour, H., Janghorban, M., & Civalek, Ö. (2020). Analysis of functionally graded doubly-curved shells with different materials via higher order shear deformation theory. *Composite Structures, 251*, Article 112645.

Aminipour, H., Janghorban, M., & Li, L. (2018). A new model for wave propagation in functionally graded anisotropic doubly-curved shells. *Composite Structures, 190*, 91–111.

Arefi, M. (2018). Analysis of a doubly curved piezoelectric nano shell: Nonlocal electro-elastic bending solution. *European Journal of Mechanics - A/Solids, 70*, 226–237.

Arefi, M. (2020). Electro-mechanical vibration characteristics of piezoelectric nano shells. *Thin-Walled Structures, 155*, Article 106912.

Arefi, M., & Amabili, M. (2021). A comprehensive electro-magneto-elastic buckling and bending analyses of three-layered doubly curved nanoshell, based on nonlocal three-dimensional theory. *Composite Structures, 257*, Article 113100.

Arefi, M., Bidgoli, E. M-R., & Civalek, Ö. (2022). Bending response of FG composite doubly curved nanoshells with thickness stretching via higher order sinusoidal shear theory. *Mechanics Based Design of Structures and Machines, 50*, 2350–2378.

Arefi, M., & Rabczuk, T. (2019). A nonlocal higher order shear deformation theory for electro-elastic analysis of a piezoelectric doubly curved nano shell. *Composites Part B: Engineering, 168*, 496–510.

Askari, M., Brusa, E., & Delprete, C. (2020). Electromechanical Vibration Characteristics of Porous Bimorph and Unimorph Doubly Curved Panels. *Actuators, 9*, 7.

Barretta, R., Caporale, A., Luciano, R., & Vaccaro, M. S. (2023). Nonlocal gradient mechanics of nanobeams for non-smooth fields. *International Journal of Engineering Science, 189*, Article 103879.

Bich, D. H., Dung, D. V., & Nam, V. H. (2013). Nonlinear dynamic analysis of eccentrically stiffened imperfect functionally graded doubly curved thin shallow shells. *Composite Structures, 96*, 384–395.

Bidgoli, E. M-R., Arefi, M., & Mohammadimehr, M. (2022). Free vibration analysis of honeycomb doubly curved shell integrated with CNT-reinforced piezoelectric layers. *Mechanics Based Design of Structures and Machines, 50*, 4409–4440.
Biswas, M., & Sanjeev, A. S. (2023). Plane wave reflection in micro-structural piezomagnetic-flexomagnetic solid with impedance boundary conditions. *Mechanics Based Design of Structures and Machines*. https://doi.org/10.1080/15397734.2023.2297256
Biswas, M., & Sanjeev, A. S. (2024). Response of surface effect on plane wave reflection at the boundary of flexomagnetic substrate. *Mechanics of Advanced Materials and Structures*. https://doi.org/10.1080/15376494.2024.2303384
Cao, Y., Khorami, M., Baharom, Sh., Assilzadeh, H., & Dindarloo, M. H. (2021). The effects of multi-directional functionally graded materials on the natural frequency of the doubly-curved nanoshells. *Composite Structures, 258*, Article 113403.
Civalek, Ö. (2005). Geometrically nonlinear dynamic analysis of doubly curved isotropic shells resting on elastic foundation by a combination of harmonic differential quadrature-finite difference methods. *International Journal of Pressure Vessels and Piping, 82*, 470–479.
Civalek, Ö., Uzun, B., & Özgür Yaylı, M. (2023). On nonlinear stability analysis of saturated embedded porous nanobeams. *International Journal of Engineering Science, 190*, Article 103898.
Dastjerdi, S. H., & Akgöz, B. (2019). On the statics of fullerene structures. *International Journal of Engineering Science, 142*, 125–144.
Dastjerdi, S. H., Akgöz, B., & Civalek, Ö. (2020a). On the effect of viscoelasticity on behavior of gyroscopes. *International Journal of Engineering Science, 149*, Article 103236.
Dastjerdi, S. H., Akgöz, B., & Civalek, Ö. (2021a). On the shell model for human eye in Glaucoma disease. *International Journal of Engineering Science, 158*, Article 103414.
Dastjerdi, S. H., Akgöz, B., Civalek, Ö., Malikan, M., & Eremeyev, V. A. (2020b). On the non-linear dynamics of torus-shaped and cylindrical shell structures. *International Journal of Engineering Science, 156*, Article 103371.
Dastjerdi, S. H., Alibakhshi, A., Akgöz, B., & Civalek, Ö. (2023a). On a comprehensive analysis for mechanical problems of spherical structures. *International Journal of Engineering Science, 183*, Article 103796.
Dastjerdi, S. H., Civalek, Ö., Malikan, M., & Akgöz, B. (2023b). On analysis of nanocomposite conical structures. *International Journal of Engineering Science, 191*, Article 103918.
Dastjerdi, S. H., & Jabbarzadeh, M. (2016). Nonlinear bending analysis of bilayer orthotropic graphene sheets resting on Winkler–Pasternak elastic foundation based on non-local continuum mechanics. *Composites Part B: Engineering, 87*, 161–175.
Dastjerdi, S. H., Malikan, M., Akgöz, B., Civalek, Ö., Wiczenbach, T., & Eremeyev, V. A. (2022). On the deformation and frequency analyses of SARS-CoV-2 at nanoscale. *International Journal of Engineering Science, 170*, Article 103604.
Dastjerdi, S. H., Naeijian, F., Akgöz, B., & Civalek, Ö. (2021b). On the mechanical analysis of microcrystalline cellulose sheets. *International Journal of Engineering Science, 166*, Article 103500.
Dindarloo, M. H., Li, L., Dimitri, R., & Tornabene, F. (2020). Nonlocal elasticity response of doubly-curved nanoshells. *Symmetry, 12*, 466.
Duc, N. D., Hadavinia, H., Quan, T. Q., & Khoa, N. D. (2019). Free vibration and nonlinear dynamic response of imperfect nanocomposite FG-CNTRC double curved shallow shells in thermal environment. *European Journal of Mechanics - A/Solids, 75*, 355–366.
Eremeyev, V. A., Ganghoffer, J. F., Konopińska-Zmysłowska, V., & Uglov, N. S. (2020). Flexoelectricity and apparent piezoelectricity of a pantographic micro-bar. *International Journal of Engineering Science, 149*, Article 103213.
Fattaheian Dehkordi, S., & Tadi Beni, Y. (2022). Size-dependent continuum-based model of a truncated flexoelectric/flexomagnetic functionally graded conical nano/microshells. *Applied Physics A, 128*, 320.
Fazelzadeh, S. A., Rahmani, S., Ghavanloo, E., & Marzocca, P. (2019). Thermoelastic vibration of doubly-curved nano-composite shells reinforced by graphene nanoplatelets. *Journal of Thermal Stresses, 42*, 1–17.
Fazzolari, F. A., & Carrera, E. (2014). Refined hierarchical kinematics quasi-3D Ritz models for free vibration analysis of doubly curved FGM shells and sandwich shells with FGM core. *Journal of Sound and Vibration, 333*, 1485–1508.
Fu, G., Zhang, Z., Dong, C., Sun, Y., Wang, J., & Zheng, H. (2023). On the magneto-mechanical response of piezomagnetic microbeam with size effects. *Thin-Walled Structures, 191*, Article 111040.
Ghavanloo, E., & Fazelzadeh, S. A. (2013). Free vibration analysis of orthotropic doubly-curved shallow shells based on the gradient elasticity. *Composites Part B: Engineering, 45*, 1448–1457.
Ghayesh, M. H., & Farokhi, H. (2017). Nonlinear mechanics of doubly curved shallow microshells. *International Journal of Engineering Science, 119*, 288–304.
Guinovart-Sanjuán, D., Mohapatra, R., Rodríguez-Ramos, R., Espinosa-Almeyda, Y., & Rodríguez-Bermúdez, P. (2023). Influence of nonlocal elasticity tensor and flexoelectricity in a rod: An asymptotic homogenization approach. *International Journal of Engineering Science, 193*, Article 103960.
Guo, J., Shi, D., Wang, Q., Tang, J., & Shuai, C. (2018). Dynamic analysis of laminated doubly-curved shells with general boundary conditions by means of a domain decomposition method. *International Journal of Mechanical Sciences, 138–139*, 159–186.
Hao, Y., Li, Z., Zhang, W., Li, S. H. B., & Yao, M. H. (2018). Vibration of functionally graded sandwich doubly curved shells using improved shear deformation theory. *Science China Technological Sciences, 61*, 791–808.
Hrytsyna, O., Sladek, J., Sladek, V., & Hrytsyna, M. (2022). Love waves propagation in layered waveguide structures including flexomagneticity/flexoelectricity and micro-inertia effects. *Mechanics of Advanced Materials and Structures, 30*, 4933–4951.
Huang, S., & Qiao, P. (2020). A new semi-analytical method for nonlinear stability analysis of stiffened laminated composite doubly-curved shallow shells. *Composite Structures, 251*, Article 112526.
Karami, B., & Ghayesh, M. H. (2023). Vibration characteristics of sandwich microshells with porous functionally graded face sheets. *International Journal of Engineering Science, 189*, Article 103884.
Karami, B., & Ghayesh, M. H. (2024). Moving load excited dynamics of multi-layered imperfect microplates based on various micromechanical models. *International Journal of Engineering Science, 197*, Article 104017.
Karami, B., Janghorban, M., & Tounsi, A. (2020). Novel study on functionally graded anisotropic doubly curved nanoshells. *The European Physical Journal Plus, 135*, 103.
Karami, B., & Shahsavari, D. (2020). On the forced resonant vibration analysis of functionally graded polymer composite doubly-curved nanoshells reinforced with graphene-nanoplatelets. *Computer Methods in Applied Mechanics and Engineering, 359*, Article 112767.
Karami, B., Shahsavari, D., & Janghorban, M. (2019). On the dynamics of porous doubly-curved nanoshells. *International Journal of Engineering Science, 143*, 39–55.
Karimiasl, M., & Ebrahimi, F. (2019). Large amplitude vibration of viscoelastically damped multiscale composite doubly curved sandwich shell with flexible core and MR layers. *Thin-Walled Structures, 144*, Article 106128.
Karimiasl, M., Ebrahimi, F., & Mahesh, V. (2019a). Nonlinear forced vibration of smart multiscale sandwich composite doubly curved porous shell. *Thin-Walled Structures, 143*, Article 106152.
Karimiasl, M., Ebrahimi, F., & Mahesh, V. (2019b). Nonlinear free and forced vibration analysis of multiscale composite doubly curved shell embedded in shape-memory alloy fiber under hygrothermal environment. *Journal of Vibration and Control, 25*, 1945–1957.
Khaniki, H. B., & Ghayesh, M. H. (2023). Highly nonlinear hyperelastic shells: Statics and dynamics. *International Journal of Engineering Science, 183*, Article 103794.
Kiani, Y., Sadighi, M., & Eslami, M. R. (2013). Dynamic analysis and active control of smart doubly curved FGM panels. *Composite Structures, 102*, 205–216.
Kundu, C. H. K., & Han, J.-H. (2009). Vibration characteristics and snapping behavior of hygro-thermo-elastic composite doubly curved shells. *Composite Structures, 91*, 306–317.
Li, H., Pang, F., Gong, Q., & Teng, Y. (2019). Free vibration analysis of axisymmetric functionally graded doubly-curved shells with un-uniform thickness distribution based on Ritz method. *Composite Structures, 225*, Article 111145.
Li, H., Pang, F., Wang, X., Du, Y., & Chen, H. (2018b). Free vibration analysis for composite laminated doubly-curved shells of revolution by a semi analytical method. *Composite Structures, 201*, 86–111.

Li, Z. N., Hao, Y. X., Zhang, W., & Zhang, J. H. (2018a). Nonlinear transient response of functionally graded material sandwich doubly curved shallow shell using new displacement field. *Acta Mechanica Solida Sinica, 31*, 108–126.
Liew, K. M., & Lim, C. W. (1996). Vibration of doubly-curved shallow shells. *Acta Mechanica, 114*, 95–119.
Lotfan, S., Rafiei Anamagh, M., & Bediz, B. (2021). A general higher-order model for vibration analysis of axially moving doubly-curved panels/shells. *Thin-Walled Structures, 164*, Article 107813.
Lukashev, P., & Sabirianov, R. F. (2010). Flexomagnetic effect in frustrated triangular magnetic structures. *Physical Review B, 82*, Article 094417.
Mahapatra, T. R., Kar, V. R., & Panda, S. K. (2017a). Nonlinear free vibration analysis of laminated composite doubly curved shell panel in hygrothermal environment. *Journal of Sandwich Structures & Materials, 17*, 511–545.
Mahapatra, T. R., Kar, V. R., & Panda, S. K. (2017b). Nonlinear thermoelastic deflection of temperature-dependent FGM curved shallow shell under nonlinear thermal loading. *Journal of Thermal Stresses, 40*, 1184–1199.
Mahapatra, T. R., Panda, S. K., & Kar, V. R. (2016). Geometrically nonlinear flexural analysis of hygro-thermo-elastic laminated composite doubly curved shell panel. *International Journal of Mechanics and Materials in Design, 12*, 153–171.
Malikan, M., Dastjerdi, Sh., Eremeyev, V. A., & Sedighi, H. M. (2023). On a 3D material modelling of smart nanocomposite structures. *International Journal of Engineering Science, 193*, Article 103966.
Malikan, M., & Eremeyev, V.A. (2020a). Free vibration of flexomagnetic nanostructured tubes based on stress-driven nonlocal elasticity. In Analysis of shells, plates, and beams, 1st ed.; Altenbach, H., Chinchaladze, N., Kienzler R., Müller, W.H., Eds.; Springer Nature, Switzerland, Volume 134, pp. 215–226.
Malikan, M., & Eremeyev, V. A. (2020b). On the geometrically nonlinear vibration of a piezo-flexomagnetic nanotube. *Mathematical Methods in the Applied Sciences*, 1–19. https://doi.org/10.1002/mma.6758
Malikan, M., & Eremeyev, V. A. (2020c). On nonlinear bending study of a piezo-flexomagnetic nanobeam based on an analytical-numerical solution. *Nanomaterials, 10*, 1–22.
Malikan, M., & Eremeyev, V. A. (2020d). On the Dynamics of a Visco–Piezo–Flexoelectric Nanobeam. *Symmetry, 12*, 643.
Malikan, M., & Eremeyev, V. A. (2021a). Effect of surface on the flexomagnetic response of ferroic composite nanostructures; nonlinear bending analysis. *Composite Structures, 271*, Article 114179.
Malikan, M., & Eremeyev, V. A. (2021b). Flexomagnetic response of buckled piezomagnetic composite nanoplates. *Composite Structures, 267*, Article 113932.
Malikan, M., & Eremeyev, V. A. (2022a). Flexomagneticity in buckled shear deformable hard-magnetic soft structures. *Continuum Mechanics and Thermodynamics, 34*, 1–16.
Malikan, M., & Eremeyev, V. A. (2022b). The effect of shear deformations' rotary inertia on the vibrating response of multi-physic composite beam-like actuators. *Composite Structures, 297*, Article 115951.
Malikan, M., & Eremeyev, V. A. (2022c). On a flexomagnetic behavior of composite structures. *International Journal of Engineering Science, 175*, Article 103671.
Malikan, M., & Eremeyev, V. A. (2023). On dynamic modeling of piezomagnetic/flexomagnetic microstructures based on Lord–Shulman thermoelastic model. *Archive of Applied Mechanics, 93*, 181–196.
Malikan, M., Eremeyev, V. A., & Sedighi, H. M. (2020a). Buckling analysis of a non-concentric double-walled carbon nanotube. *Acta Mechanica, 231*, 5007–5020.
Malikan, M., Eremeyev, V. A., & Żur, K. K. (2020b). Effect of Axial Porosities on Flexomagnetic Response of In-Plane Compressed Piezomagnetic Nanobeams. *Symmetry, 12*, 1935. Article.
Malikan, M., & Nguyen, V. B. (2018). Buckling analysis of piezo-magnetoelectric nanoplates in hygrothermal environment based on a novel one variable plate theory combining with higher-order nonlocal strain gradient theory. *Physica E: Low-dimensional Systems and Nanostructures, 102*, 8–28.
Malikan, M., Nguyen, V. B., Dimitri, R., & Tornabene, F. (2019). Dynamic modeling of non-cylindrical curved viscoelastic single-walled carbon nanotubes based on the second gradient theory. *Materials Research Express, 6*, Article 075041.
Malikan, M., & Sadraee Far, M. N. (2018). Differential Quadrature Method for Dynamic Buckling of Graphene Sheet Coupled by a Viscoelastic Medium Using Neperian Frequency Based on Nonlocal Elasticity Theory. *Journal of Applied and Computational Mechanics, 4*, 147–160.
Malikan, M., Uglov, N. S., & Eremeyev, V. A. (2020c). On instabilities and post-buckling of piezomagnetic and flexomagnetic nanostructures. *International Journal of Engineering Science, 157*, Article 103395.
Malikan, M., Wiczenbach, T., & Eremeyev, V. A. (2021). On thermal stability of piezo-flexomagnetic microbeams considering different temperature distributions. *Continuum Mechanics and Thermodynamics, 33*, 1281–1297.
Malikan, M., Wiczenbach, T., & Eremeyev, V. A. (2022). Thermal buckling of functionally graded piezomagnetic micro- and nanobeams presenting the flexomagnetic effect. *Continuum Mechanics and Thermodynamics, 34*, 1051–1066.
Mawassy, N., Reda, H., Ganghoffer, J. F., Eremeyev, V. A., & Lakiss, H. (2021). A variational approach of homogenization of piezoelectric composites towards piezoelectric and flexoelectric effective media. *International Journal of Engineering Science, 158*, Article 103410.
Mehar, K., Mishra, P. K., & Panda, S. K. (2021). Thermal buckling strength of smart nanotube-reinforced doubly curved hybrid composite panels. *Computers & Mathematics with Applications, 90*, 13–24.
Momeni-Khabisi, H., & Tahani, M. (2023). Coupled thermal stability analysis of piezomagnetic nano-sensors and nano-actuators considering the flexomagnetic effect. *European Journal of Mechanics - A/Solids, 97*, Article 104773.
Momeni-Khabisi, H., & Tahani, M. (2024). Buckling and post-buckling analysis of double-layer magnetoelectric nano-plate strips considering piezo-flexoelectric and piezo-flexomagnetic effects. *European Journal of Mechanics - A/Solids, 104*, Article 105218.
Monge, J. C., & Mantari, J. L. (2020). Exact solution of thermo-mechanical analysis of laminated composite and sandwich doubly-curved shell. *Composite Structures, 245*, Article 112323.
Nath Thakur, S., & Ray, Ch. (2021). Transient dynamic response of doubly curved laminated composite shells under pulse loading. *Thin-Walled Structures, 160*, Article 107342.
Pouresmaeeli, S., & Fazelzadeh, S. A. (2016). Frequency analysis of doubly curved functionally graded carbon nanotube-reinforced composite panels. *Acta Mechanica, 227*, 2765–2794.
Reddy, J. N. (2003). *Mechanics of laminated composite plates and shells: Theory and analysis*. CRC Press.
Reddy, J. N., & Asce, M. (1984). Exact solutions of moderately thick laminated shells. *Journal of Engineering Mechanics, 110*, 794–809.
Reddy, J. N., & Liu, C. F. (1985). A higher-order shear deformation theory of laminated elastic shells. *International Journal of Engineering Science, 23*, 319–330.
Sayyad, A. S., & Ghugal, Y. M. (2021). Static and free vibration analysis of doubly-curved functionally graded material shells. *Composite Structures, 269*, Article 114045.
Shahmohammadi, M. A., Abdollahi, P., & Salehipour, H. (2022). Geometrically nonlinear analysis of doubly curved imperfect shallow shells made of functionally graded carbon nanotube reinforced composite (FG_CNTRC). *Mechanics Based Design of Structures and Machines, 50*, 3796–3820.
Shahmohammadi, M. A., Mirfatah, S. M., Salehipour, H., & Civalek, Ö. (2023). On nonlinear forced vibration of micro scaled panels. *International Journal of Engineering Science, 182*, Article 103774.
Sidhardh, S., & Ray, M. C. (2018). Flexomagnetic response of nanostructures. *Journal of Applied Physics, 124*, Article 244101.
Singh, V. K., & Panda, S. K. (2014). Nonlinear free vibration analysis of single/doubly curved composite shallow shell panels. *Thin-Walled Structures, 85*, 341–349.
Singh, V. K., & Panda, S. K. (2017). Geometrical nonlinear free vibration analysis of laminated composite doubly curved shell panels embedded with piezoelectric layers. *Journal of Vibration and Control, 23*, 2078–2093.
Sladek, J., Sladek, V., Xu, M., & Deng, Q. (2021). A cantilever beam analysis with flexomagnetic effect. *Meccanica, 56*, 2281–2292.
Sobhy, M. (2018). Magneto-electro-thermal bending of FG-graphene reinforced polymer doubly-curved shallow shells with piezoelectromagnetic faces. *Composite Structures, 203*, 844–860.
Sofiyev, A. H. (2023). Nonlinear forced response of doubly-curved laminated panels composed of cnt patterned layers within first order shear deformation theory. *Thin-Walled Structures, 193*, Article 111227.

Stempin, P., Pawlak, T. P., & Sumelka, W. (2023). Formulation of non-local space-fractional plate model and validation for composite micro-plates. *International Journal of Engineering Science, 192*, Article 103932.
Stempin, P., & Sumelka, W. (2022). Space-fractional small-strain plasticity model for microbeams including grain size effect. *International Journal of Engineering Science, 175*, Article 103672.
Thakur, S. N., Ray, C., & Chakraborty, S. (2017). A new efficient higher-order shear deformation theory for a doubly curved laminated composite shell. *Acta Mechanica, 228*, 69–87.
Tham, V. V., Quoc, T. H., & Tu, T. M. (2019). Free vibration analysis of laminated functionally graded carbon nanotube-reinforced composite doubly curved shallow shell panels using a new four-variable refined theory. *Journal of Composites Science, 3*, 104.
Tornabene, F. (2011). 2-D GDQ solution for free vibrations of anisotropic doubly-curved shells and panels of revolution. *Composite Structures, 93*, 1854–1876.
Tornabene, F. (2016). General higher order layer-wise theory for free vibrations of doubly-curved laminated composite shells and panels. *Mechanics of Advanced Materials and Structures, 23*, 1046–1067.
Tornabene, F. (2019). On the critical speed evaluation of arbitrarily oriented rotating doubly-curved shells made of functionally graded materials. *Thin-Walled Structures, 140*, 85–98.
Tornabene, F., & Bacciocchi, M. (2018). Dynamic stability of doubly-curved multilayered shells subjected to arbitrarily oriented angular velocities: Numerical evaluation of the critical speed. *Composite Structures, 201*, 1031–1055.
Tornabene, F., & Brischetto, S. (2018). 3D capability of refined GDQ models for the bending analysis of composite and sandwich plates, spherical and doubly-curved shells. *Thin-Walled Structures, 129*, 94–124.
Tornabene, F., Fantuzzi, N., & Bacciocchi, M. (2014). The local GDQ method applied to general higher-order theories of doubly-curved laminated composite shells and panels: The free vibration analysis. *Composite Structures, 116*, 637–660.
Tornabene, F., Fantuzzi, N., & Bacciocchi, M. (2016). On the mechanics of laminated doubly-curved shells subjected to point and line loads. *International Journal of Engineering Science, 109*, 115–164.
Tornabene, F., Fantuzzi, N., & Bacciocchi, M. (2017). A new doubly-curved shell element for the free vibrations of arbitrarily shaped laminated structures based on Weak Formulation IsoGeometric Analysis. *Composite Structures, 171*, 429–461.
Tornabene, F., Fantuzzi, N., Bacciocchi, M., & Viola, E. (2015). Higher-order theories for the free vibrations of doubly-curved laminated panels with curvilinear reinforcing fibers by means of a local version of the GDQ method. *Composites Part B: Engineering, 81*, 196–230.
Tornabene, F., Liverani, A., & Caligiana, G. (2012). General anisotropic doubly-curved shell theory: A differential quadrature solution for free vibrations of shells and panels of revolution with a free-form meridian. *Journal of Sound and Vibration, 331*, 4848–4869.
Tornabene, F., & Viola, E. (2013). Static analysis of functionally graded doubly-curved shells and panels of revolution. *Meccanica, 48*, 901–930.
Tornabene, F., Viola, E., & Fantuzzi, N. (2013). General higher-order equivalent single layer theory for free vibrations of doubly-curved laminated composite shells and panels. *Composite Structures, 104*, 94–117.
Tornabene, F., Viscoti, M., & Dimitri, R. (2023). Free vibration analysis of laminated doubly-curved shells with arbitrary material orientation distribution employing higher order theories and differential quadrature method. *Engineering Analysis with Boundary Elements, 152*, 397–445.
Tornabene, F., Viscoti, M., Dimitri, R., & Antonietta Aiello, M (2021a). Higher order formulations for doubly-curved shell structures with a honeycomb core. *Thin-Walled Structures, 164*, Article 107789.
Tornabene, F., Viscoti, M., Dimitri, R., & Reddy, J. N. (2021b). Higher order theories for the vibration study of doubly-curved anisotropic shells with a variable thickness and isogeometric mapped geometry. *Composite Structures, 267*, Article 113829.
Tran, Q. H., Duong, H. T., & Tran, T. M. (2018). Free vibration analysis of functionally graded doubly curved shell panels resting on elastic foundation in thermal environment. *International Journal of Advanced Structural Engineering, 10*, 275–283.
Tsai, Y.-H., Wu, C.-P., & Syu, Y.-S. (2008). Three-dimensional analysis of doubly curved functionally graded magneto-electro-elastic shells. *European Journal of Mechanics - A/Solids, 27*, 79–105.
Vinyas, M., & Harursampath, D. (2020). Nonlinear vibrations of magneto-electro-elastic doubly curved shells reinforced with carbon nanotubes. *Composite Structures, 253*, Article 112749.
Viola, E., Tornabene, F., & Fantuzzi, N. (2013). Static analysis of completely doubly-curved laminated shells and panels using general higher-order shear deformation theories. *Composite Structures, 101*, 59–93.
Wang, A., Chen, H., Hao, Y., & Zhang, W. (2018). Vibration and bending behavior of functionally graded nanocomposite doubly-curved shallow shells reinforced by graphene nanoplatelets. *Results in Physics, 9*, 550–559.
Wang, Q., Cui, X., Qin, B., Liang, Q., & Tang, J. (2017). A semi-analytical method for vibration analysis of functionally graded (FG) sandwich doubly-curved panels and shells of revolution. *International Journal of Mechanical Sciences, 134*, 479–499.
Xu, X., Shahsavari, D., & Karami, B. (2021). On the forced mechanics of doubly-curved nanoshell. *International Journal of Engineering Science, 168*, Article 103538.
Zamani, H. A. (2021). Free vibration of doubly-curved generally laminated composite panels with viscoelastic matrix. *Composite Structures, 258*, Article 113311.
Zare Jouneghani, F., Dimitri, R., Bacciocchi, M., & Tornabene, F. (2017). Free vibration analysis of functionally graded porous doubly-curved shells based on the first-order shear deformation theory. *Applied Sciences, 7*, 1252.
Zhang, N., Zheng, S., & Chen, D. (2019). Size-dependent static bending of flexomagnetic nanobeams. *Journal of Applied Physics, 126*, Article 223901.
Zhou, Y. Y., Lü, C. F., & Chen, W. Q. (2012). Bulk wave propagation in layered piezomagnetic/piezoelectric plates with initial stresses or interface imperfections. *Composite Structures, 94*, 2736–2745.
Zhu, C., Fang, X., & Nie, G. (2021). Nonlinear free and forced vibration of porous piezoelectric doubly-curved shells based on NUEF model. *Thin-Walled Structures, 163*, Article 107678.
Zhu, C., Fang, X., & Yang, S. (2019). Nonlinear free vibration of functionally graded viscoelastic piezoelectric doubly curved nanoshells with surface effects. *The European Physical Journal Plus, 134*, 486.